

Best of Both Worlds: Multimodal Reasoning and Generation via Unified Discrete Flow Matching

Onkar Susladkar[♦] Tushar Prakash[♦] Gayatri Deshmukh[♦] Kiet A. Nguyen[♦] Jiaxun Zhang[♦]
 Adheesh Juvekar[♦] Tianshu Bao[♦] Lin Chai[♦] Sparsh Mittal[♦] Inderjit S Dhillon[♦] Ismini Lourentzou[♦]
[♦]University of Illinois Urbana-Champaign [♦]Independent Researcher [♦]Indian Institute of Technology Roorkee
[♦]University of Texas at Austin [♦]Google



Figure 1: We propose UniDFlow a unified multimodal diffusion framework that supports image understanding, generation, and thinking-based editing. The model performs visual reasoning for question answering, produces high-quality text-to-image generations across diverse scenes and subjects, and enables instruction-driven, multi-step image editing through structured reasoning.

Abstract. We propose UniDFlow, a unified discrete flow-matching framework for multimodal understanding, generation, and editing. It decouples understanding and generation via task-specific low-rank adapters, avoiding objective interference and representation entanglement, while a novel reference-based multimodal preference alignment optimizes relative outcomes under identical conditioning, improving faithfulness and controllability without large-scale retraining. UniDFlow achieves SOTA performance across eight benchmarks and exhibits strong zero-shot generalization to tasks including inpainting, in-context image generation, reference-based editing, and compositional generation, despite no explicit task-specific training.

<https://plan-lab.github.io/unidflow>



1. Introduction

Multimodal generative systems have become central to everyday productivity, with large language models (LLMs) such as ChatGPT [39] and Gemini [58] enabling strong reasoning and instruction following. Similarly, diffusion-based models such as Stable

Diffusion [15, 45] and DALL·E [6, 44] excel at high-fidelity image and video generation. However, these models remain largely disjoint as LLM-centric models excel at understanding but lack native generative mechanisms, while diffusion models provide powerful generation with limited semantic grounding and reasoning. This separation motivates

unified multimodal models that integrate LLM-level understanding with diffusion-level generation within a single architecture [63, 68].

Early approaches in this direction, such as Emu [13] and Chameleon [57], represent images as visual tokens and model both text and vision using a single auto-regressive (AR) transformer [61]. While simple, AR-based generation is highly inefficient for high-dimensional visual outputs. Hybrid models, including EMMA [24], OmniGen2 [65], Mammoth-Moda2 [48], and BAGEL [14], combine AR modeling for text with diffusion-style objectives for images to retain language understanding while improving generation. Moreover, UniDisc [55] and Mudit [50] employ fully discrete diffusion with a unified denoising objective for text and images, but performance lags behind hybrid models.

Despite recent progress, existing unified models still face several fundamental limitations. (1) Large-scale AR-diffusion frameworks couple cross-entropy decoding with diffusion-style regression [48, 65], creating mismatched objectives that lead to unstable joint optimization. (2) Even with strong pretrained initialization, many approaches rely on full-model updates over hundreds of millions of samples [14, 24], incurring substantial compute while often degrading general-purpose reasoning ability. (3) Current unified diffusion approaches entangle understanding and generation within shared parameters, thus improving one capability can inadvertently erode the other [50, 78]. (4) Generation and editing are often improved through additional alignment stages, such as multimodal reflection [65] or reinforcement learning with scalar rewards [48]. However, these approaches optimize outputs in isolation, encouraging higher scores or improved reasoning trajectories without modeling relative preference under identical conditioning. As a result, they fail to learn explicit decision boundaries between faithful and subtly incorrect edits.

To address the aforementioned limitations, we introduce UniDFlow, a unified discrete diffusion framework for efficient multimodal understanding and generation. UniDFlow leverages a strong pretrained vision-language model as a prior, avoiding redundant



Figure 2: Instruction-guided editing attention maps showing UniDFlow more precisely focuses on relevant regions than prior models.

pretraining and enabling parameter-efficient adaptation through lightweight adapters. We perform large-scale three-stage training: (i) an understanding-focused stage, (ii) a generation-focused stage, and (iii) a joint understanding-generation stage with reference-based multimodal preference optimization to improve editing fidelity and controllability. To prevent parameter entangle, UniDFlow trains separate adapters for understanding and generation, while the final stage trains only a lightweight router to combine them dynamically

Fig. 2 visualizes the instruction-guided activation maps during editing. UniDFlow consistently attends more precisely to instruction-relevant regions, whether modifying coarse objects (e.g., adding a T-shirt) or finer details (e.g., changing the swoosh color). Our main contributions are:

- We introduce UniDFlow, a unified discrete diffusion model that repurposes a pretrained vision-language backbone as a generator over multimodal tokens, enabling understanding, text generation, image synthesis, and editing within one probabilistic interface.
- We unify text and image generation under a single discrete flow-matching objective for all tasks and incorporate a stable time-conditioning mechanism that preserves the backbone’s reasoning priors. Compared to prior multi-objectives, UniDFlow achieves efficient training and inference, requiring only 20 denoising steps while preserving high generation quality.

- We propose mRefDPO, a reference-guided multi-modal preference alignment that optimizes relative preferences conditioned on both the instruction and the visual reference, leading to more faithful and controllable editing.
- UniDFlow achieves state-of-the-art performance on 8 benchmarks spanning understanding, generation, and editing, with up to 13% improvement over larger unified models with more than 3 \times parameters, and up to 24% gains over popular models such as Qwen 3 [5] and DeepSeek-VL2 [67].

2. Related Work

Diffusion for Visual Generation. Diffusion probabilistic models (DPMs) [25, 38, 46] outperform GANs [22] in stability and quality but are costly in pixel space. Latent diffusion models (LDMs) [45] mitigate this via compressed latent representations, enabling strong text-to-image generation [9, 41, 77]. Discrete diffusion [2] extends diffusion to categorical spaces using masking-based corruption, motivating parallel mask-and-predict generators that improve fidelity and efficiency [8, 23].

Unified Models for Understanding and Generation. To unify understanding and generation, early works such as Emu [13, 52] and Chameleon [57] adopt fully autoregressive modeling over text and visual tokens, but scale poorly for high-resolution images. Hybrid frameworks, including EMMA [24], Omni-Gen2 [65], MammothModa2 [48], and BAGEL [14], combine autoregressive text modeling with diffusion-based image generation, yet still face modality and objective mismatches. Fully discrete diffusion models such as UniDisc [55] and Muddit [50] further unify modeling but lag behind large-scale hybrids. Our work introduces UniDFlow, a unified discrete flow-matching model with stable time-conditioning that preserves reasoning priors and enables efficient, high-fidelity multimodal generation and editing.

LLM and Diffusion Preference Alignment. LLMs [31, 60] provide strong reasoning with autoregressive Transformers, and VLMs [3] extend them to images by projecting visual features (e.g., SigLIP [76]) into the language token space. Models

such as Qwen [5], LLaVA [32], BLIP-2 [29], and Flamingo [1] excel at multimodal understanding but typically rely on separate diffusion backbones for image generation and editing. Preference learning has also been adapted to diffusion models, including Diffusion-DPO [62], score-space alignment (DSPO) [79], and stabilized variants such as DGPO [37] and discrete-diffusion extensions [7]. Prior work further improves controllability via additional alignment stages (e.g., multimodal reflection [65] or scalar-reward RL [48]). In contrast, UniDFlow performs *reference-based multimodal preference alignment*, optimizing a pairwise log-likelihood margin against a frozen reference model for stable, comparative supervision, improving faithfulness and controllable editing.

3. Method

3.1. Preliminaries: Discrete Flow Matching

We use Discrete Flow Matching (DFM) [19] as the common objective across all training stages. DFM learns a transport field in discrete spaces by mapping samples from noise to data. Let $x_0 \sim q_{\text{data}}$ denote a clean discrete sample (e.g., text or visual tokens), and x_t its corrupted version at time step $t \in \{0, \dots, T\}$ generated by a fixed forward noising process $q(x_t \mid x_0, t)$. Given x_t , a flow network $f_\theta(x_t, t, c)$ conditioned on time t and context c predicts the transport toward the clean state as $f_\theta(x_t, t, c) \approx q(x_0 \mid x_t, t, c)$. The model is trained by minimizing a token-wise categorical negative log-likelihood:

$$\mathcal{L}_{\text{DFM}}(\theta; x_0 \mid x_t, t, c) = \mathbb{E}_{x_0, t, x_t} [-\log f_\theta(x_0 \mid x_t, t, c)]. \quad (1)$$

At inference, sampling starts from $x_T \sim q_{\text{noise}}$ and applies the learned flow to recover x_0 . By directly estimating transport directions, DFM enables efficient few-step sampling, with conditioning via context c supporting unified language modeling, visual generation, and editing.

3.2. UniDFlow

We cast multimodal understanding, conditional generation, and instruction-based image editing as a single discrete denoising process. Starting

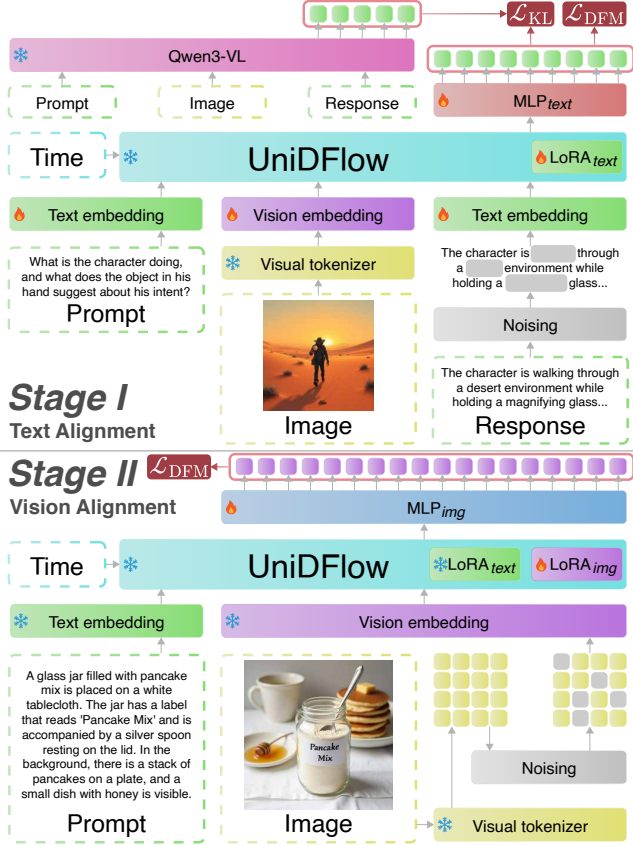


Figure 3: Overview of Stage I (understanding via text alignment) and Stage II (generation via vision alignment) of UniDFlow.

from a pretrained vision–language transformer with parameters θ_0 , UniDFlow learns to recover a clean token sequence from a corrupted one under appropriate conditioning. For understanding, the denoised sequence corresponds to answer text tokens conditioned on an instruction p and an input image x ; for generation and editing, it corresponds to visual tokens conditioned on p and a reference image x_{ref} . To enable discrete diffusion over images, we map images to sequences of discrete visual tokens using a pretrained tokenizer, and we use bidirectional self-attention to support full-context denoising. All task-specific adaptation is implemented with low-rank adapters (LoRA), while θ_0 remains frozen.

Our training follows a three-stage pipeline (illustrated in Figs. 3 and 4): Stage I aligns the pretrained vision–language backbone for diffusion-based multimodal understanding, Stage II adapts the model for discrete visual generation while preserving

reasoning capabilities, and Stage III performs reference-based multimodal preference alignment to improve fidelity and controllability. We first describe the time-conditioned normalization used throughout the model, followed by the three training stages.

3.2.1. Time-Step Guided RMSNorm

Conditioning a pretrained transformer on diffusion time by directly adding time embeddings to attention or MLP activations can destabilize training by perturbing learned feature distributions. We address this with Time-Step Guided RMSNorm (TSG-RMSNorm), which injects time information by modulating the RMSNorm scale parameters rather than altering the activations themselves. This preserves pretrained representations by keeping the direction of hidden states unchanged while only applying a controlled, time-dependent rescaling.

Let $h_\ell \in \mathbb{R}^d$ denote the input hidden state (activation vector) to the RMSNorm layer at transformer layer ℓ . Standard RMSNorm is $\text{RMSNorm}(h_\ell) = \gamma_\ell \odot \frac{h_\ell}{\text{RMS}(h_\ell)}$, where $\text{RMS}(h_\ell) = \sqrt{\frac{1}{d} \sum_{j=1}^d h_{\ell,j}^2 + \varepsilon}$. Given a time embedding $e(t)$, we predict a time-dependent modulation for each layer, *i.e.*, $s_\ell(t) = W_\ell^{(s)} e(t)$, $b_\ell(t) = W_\ell^{(b)} e(t)$. We apply these to the pretrained RMSNorm parameters via

$$\begin{aligned} \text{TSG-RMSNorm}(h_\ell, t) &= \text{RMSNorm}(h_\ell) \\ &\odot (\gamma_\ell \odot (1 + s_\ell(t))) + b_\ell(t), \end{aligned} \quad (2)$$

where γ_ℓ is the pretrained RMSNorm scale and \odot denotes element-wise multiplication. All time-modulation parameters are zero-initialized so that $s_\ell(t) = 0$ and $b_\ell(t) = 0$ at initialization, exactly recovering the pretrained model.

3.2.2. Stage I: Text Alignment

Unified multimodal models often entangle understanding and generation objectives, leading to representational interference and degraded reasoning. We first adapt the pretrained backbone to diffusion-style understanding through text alignment in isolation, preserving language–visual reasoning before introducing generative training.

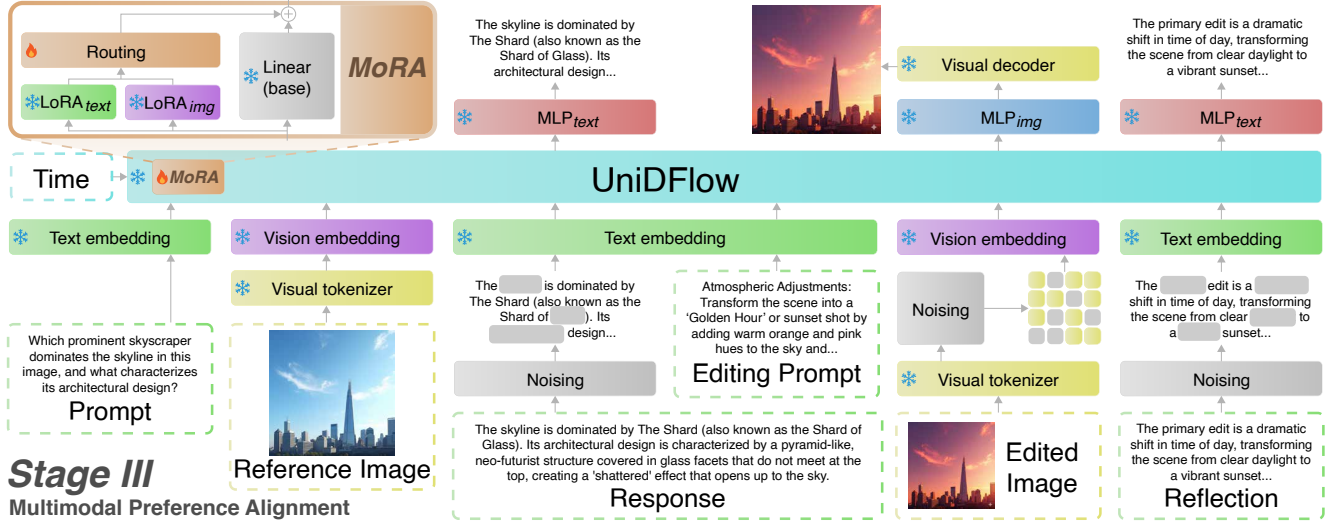


Figure 4: Stage III of UniDFlow: reference-based multimodal preference alignment for improved faithfulness, controllability, and editing.

Given an instruction p , visual tokens x , and a fully masked text token sequence $y_{\text{txt},t}$, the model predicts the clean answer tokens $y_{\text{txt},0}$ using discrete flow matching. The training objective follows Eq. 1:

$$\mathcal{L}_{\text{under}} = \mathcal{L}_{\text{DFM}}(\Delta\theta_u; y_{\text{txt},0} | y_{\text{txt},t}, p, x), \quad (3)$$

where θ_0 denotes frozen pretrained VLM parameters and $\Delta\theta_u$ are $LoRA_{\text{text}}$ adapters specialized for understanding. To prevent semantic drift from the pretrained language behavior, we additionally regularize the diffusion-predicted distribution with a KL divergence against the autoregressive answer distribution produced by the original VLM:

$$\mathcal{L}_{\text{KL}} = \text{KL}\left(p_{\text{DFM}}(y_{\text{txt},0} | y_{\text{txt},t}, t, p, x) \parallel p_{\text{PAR}}(y_{\text{txt}} | p, x)\right). \quad (4)$$

This constraint anchors diffusion decoding to the pretrained linguistic manifold while allowing bidirectional attention and time-conditioned normalization to support non-autoregressive reasoning. The total Stage I objective is $\mathcal{L}_{\text{Stage I}} = \mathcal{L}_{\text{under}} + \lambda_{\text{KL}} \mathcal{L}_{\text{KL}}$.

3.2.3. Stage II: Vision Alignment

This stage adapts the same frozen backbone for conditional generation in a discrete visual token space, while preserving the understanding behavior learned in the previous training stage. We keep θ_0 and $\Delta\theta_u$ frozen and introduce a separate set of LoRA adapters $\Delta\theta_g$ specialized for generation.

Given an instruction p and corrupted visual tokens $y_{\text{vis},t}$, the model predicts clean visual tokens $y_{\text{vis},0}$ using discrete flow matching:

$$\mathcal{L}_{\text{Stage II}} = \mathcal{L}_{\text{DFM}}(\Delta\theta_g; y_{\text{vis},0} | y_{\text{vis},t}, t, p), \quad (5)$$

where only $\Delta\theta_g$ ($LoRA_{\text{img}}$) is trainable, while θ_0 and the understanding adapters $\Delta\theta_u$ are kept frozen. The diffusion process operates entirely in a discrete latent space, enabling efficient sampling and seamless integration with the backbone’s token-based architecture. By isolating generation-specific parameters, Stage II establishes strong conditional image generation capabilities without interfering with the language and reasoning behavior learned during Stage I.

3.2.4. Stage III: Reference-Based Multimodal Preference Alignment

While the previous stages endow UniDFlow with strong multimodal understanding and generation capabilities, token-level likelihood training cannot reliably distinguish between multiple plausible outputs that differ in instruction fidelity, visual grounding, or reasoning consistency. Stage III therefore introduces a reference-based multimodal preference alignment objective that explicitly optimizes relative preferences across text, vision, and reflection, grounded in reference images.

Each preference instance specifies an instruction p with paired preferred(w)/rejected(l) outcomes: reference image ($x_{\text{ref}}^w, x_{\text{ref}}^l$), text responses ($y_{\text{txt}}^w, y_{\text{txt}}^l$), visual tokens ($y_{\text{vis}}^w, y_{\text{vis}}^l$), and reflection sequences (r^w, r^l). This formulation allows the model to learn which multimodal outcomes are preferred, conditioned on both the instruction and the reference.

Mixture-of-LoRA Routing (MoRA). Since this stage optimizes preferences for both understanding and generation, naively sharing parameters can introduce objective interference, while static routing restricts adaptability. Therefore, we learn a lightweight router r_ϕ with parameters ϕ that dynamically composes task-specific adapters based on the hidden state at diffusion step t :

$$\Delta\theta(t) = \alpha_t \Delta\theta_u + (1 - \alpha_t) \Delta\theta_g, \quad \alpha_t = r_\phi(h_t). \quad (6)$$

Multimodal Preference Learning. We adopt a reference-anchored Direct Preference Optimization (DPO) objective with a frozen reference policy π_{ref} . For text, the loss is $\mathcal{L}_{\text{tRef-DPO}} = -\log \sigma(\beta \Delta_\theta^{\text{txt}})$ and preference margin is

$$\Delta_\theta^{\text{txt}} = \log \frac{\pi_\theta(y_{\text{txt}}^w | p, x_{\text{ref}}^w)}{\pi_{\text{ref}}(y_{\text{txt}}^w | p, x_{\text{ref}}^w)} - \log \frac{\pi_\theta(y_{\text{txt}}^l | p, x_{\text{ref}}^l)}{\pi_{\text{ref}}(y_{\text{txt}}^l | p, x_{\text{ref}}^l)}. \quad (7)$$

For vision, we concatenate reflection and image tokens as $\tilde{y}_{\text{vis}} = (r, y_{\text{vis}})$, with the loss defined as $\mathcal{L}_{\text{vRef-DPO}} = -\log \sigma(\beta \Delta_\theta^{\text{vis}})$ and preference margin

$$\Delta_\theta^{\text{vis}} = \log \frac{\pi_\theta(\tilde{y}_{\text{vis}}^w | p, x_{\text{ref}}^w)}{\pi_{\text{ref}}(\tilde{y}_{\text{vis}}^w | p, x_{\text{ref}}^w)} - \log \frac{\pi_\theta(\tilde{y}_{\text{vis}}^l | p, x_{\text{ref}}^l)}{\pi_{\text{ref}}(\tilde{y}_{\text{vis}}^l | p, x_{\text{ref}}^l)}. \quad (8)$$

Stage III jointly aligns text and vision through a preference-augmented objective: $\mathcal{L}_{\text{mRef-DPO}} = \lambda_t \mathcal{L}_{\text{tRef-DPO}} + \lambda_v \mathcal{L}_{\text{vRef-DPO}}$, promoting faithful instruction following, grounded visual editing, and consistent multimodal behavior. We optimize a unified objective that combines discrete flow-matching (DFM) likelihood training for three output streams: (1) text generation, $\mathcal{L}_{\text{text}} = \mathcal{L}_{\text{DFM}}(\phi; y_{\text{txt},0}^w | y_{\text{txt},t}^w, x_{\text{ref}}^w, p, t)$, (2) visual editing $\mathcal{L}_{\text{edit}} = \mathcal{L}_{\text{DFM}}(\phi; y_{\text{txt},0}^w | y_{\text{vis},t}^w, x_{\text{ref}}^w, p, t)$, and (3) reflection $\mathcal{L}_{\text{refl}} = \mathcal{L}_{\text{DFM}}(\phi; r_0^w | r_t^w, x_{\text{ref}}^w, y_{\text{vis},t}^w, y_{\text{txt},t}^w, p, p_{\text{edit}}, t)$. The final objective for stage III is:

$$\mathcal{L}_{\text{Stage-III}} = \mathcal{L}_{\text{text}} + \mathcal{L}_{\text{edit}} + \mathcal{L}_{\text{refl}} + \mathcal{L}_{\text{mRef-DPO}} \quad (9)$$

The DFM terms maximize time-conditioned token likelihood along the discrete diffusion trajectory

under their respective conditionings (instruction, reference image, or edit prompt), enforcing token-level consistency. The $\mathcal{L}_{\text{mRef-DPO}}$ term introduces comparative alignment by increasing the log-likelihood margin of preferred over rejected outputs relative to a frozen reference policy π_{ref} , stabilizing training and improving cross-modal faithfulness.

4. Experiments

We conduct extensive experiments to evaluate the performance of UniDFlow across six benchmarks, covering multimodal understanding, generation, and editing. In Stage I, we train using MMINSTRUCT [34] to establish strong multimodal understanding. Stage II focuses on generative capability by training on TEXT-TO-IMAGE-4M [27, 47, 51]. Stage III performs reference-based multimodal preference alignment with 3.5M curated preference samples under identical inputs and reference images. Dataset curation for preference alignment, training, and implementation details are provided in Appendices A-B.

4.1. Multi-Modal Understanding

Table 1 reports results on the EVALVLM benchmark. Compared to strong unified hybrid baselines such as BAGEL (7B MoT), UniDFlow achieves a +6.9% improvement on MME-P and +7.0% on MME-S, indicating stronger perceptual and reasoning consistency. Against EMMA (4B), UniDFlow further improves MM-Bench by +6.3% and MathVista by +13.3%, demonstrating superior mathematical and multi-step reasoning despite comparable model scale. Moreover, compared to the unified diffusion baseline Mudit, UniDFlow achieves an overall improvement of 12% across different understanding tasks. Finally, when compared with leading understanding-only models such as Qwen2.5-VL (7B) UniDFlow attains 20.4% higher overall performance. Additional results on OCRBENCHV2 [18] can be found in Appendix D. Fig. 5 shows reasoning-based text generation examples, where UniDFlow accurately extracts information from images to respond to user queries.

Model	Params	MME-P	MME-S	MMBENCH	MMMU	MM-VET	MATHVISTA	MMVP
Qwen2.5-VL [4]	3B	–	2157	79.1	53.1	61.8	62.3	–
BLIP-3 [69]	4B	–	–	76.8	41.1	–	39.6	–
DeepSeek-VL2 [67]	4B	–	–	51.1	60.0	62.8	–	–
Qwen3-VL [5]	4B	–	–	85.1	64.1	72.5	–	–
VILA-U [66]	7B	1336	–	66.6	32.2	27.7	–	22.0
Chameleon [57]	7B	–	–	35.7	28.4	8.3	–	0.0
Janus-Pro [10]	7B	1567	–	79.2	41.0	50.0	–	–
TokenFlow-XL [20]	13B	1546	–	68.9	38.7	40.7	–	–
BAGEL [14]	7B	1687	2388	85.0	55.3	67.2	73.1	69.3
OmniGen-v2 [65]	8B	–	–	53.1	61.5	–	–	–
EMMA [24]	4B	–	–	85.8	65.1	73.0	75.8	–
MammothModa-2 [48]	4B	1753	1998	86.6	71.23	79.4	81.8	77.5
Muddit [50]	4B	1700	1832	82.8	66.6	76.2	79.1	74.1
UniDFlow	4B	1803	2555	91.2	74.3	82.7	85.9	80.2

Table 1: Comparison of multimodal understanding performance on EVALVLMBENCH [17, 35, 36, 59, 74, 75] across diverse reasoning tasks.

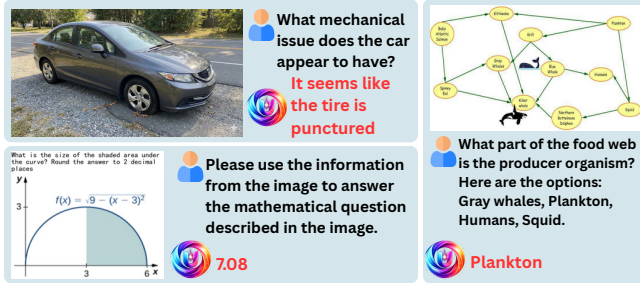


Figure 5: Multimodal reasoning from UniDFlow

4.2. Text-to-Image Generation

Table 2 summarizes the performance of UniDFlow on GENEVAL and DPGBENCH for multimodal generation. On GENEVAL, which evaluates compositional text-to-image generation across object counting, attribute binding, and spatial reasoning, UniDFlow achieves an overall score of 0.95, outperforming strong unified baselines such as EMMA and MammothModa2 by +2.2% and +9.2%, respectively, highlighting its stronger ability to associate attributes with the correct objects under compositional constraints. A similar trend is observed on DPGBENCH, which evaluates fine-grained prompt grounding across global understanding, attribute binding, and relational reasoning, where UniDFlow outperforms EMMA and MammothModa2 by +6.5% and +4.6%, respectively. Notably, UniDFlow also

Model	Params	GenEval	DPGBench
DALL-E 3 [6]	–	0.67	83.50
SD3-Medium [15]	2B	0.74	80.43
Qwen-Image(-RL) [16]	7B+20B	0.91	88.32
TokenFlow-XL [20]	14B	0.55	–
Janus-Pro-7B [10]	7B	0.80	84.19
Bagel [14]	7B+7B	0.88	87.74
OmniGen2/V2 [65]	3B+4B	0.78	83.57
MammothModa-2 [48]	8B+3B+2B	0.87	87.20
EMMA [24]	4B	0.93	85.63
MUDDIT [50]	8B	0.90	86.37
UniDFlow	4B	0.95	91.19

Table 2: Overall generation performance on GENEVAL [21] and DPGBENCH [26]. Appendix E provides full benchmark-wise breakdowns.

surpasses generation-focused models such as Qwen-Image (7B+20B) by 4.0% on GENEVAL and 3.2% on DPGBENCH, despite using substantially fewer parameters. Fig. 6 (top two rows) further demonstrates that UniDFlow produces visually faithful and prompt-consistent images, accurately rendering fine-grained details and background structures, which reflect strong global semantics and local visual fidelity.

Subject-driven generation. Furthermore, UniDFlow supports in-context subject-driven image generation from multiple reference images, as shown in Fig. 7, without any explicit task-specific training. Given reference images and a textual instruction, UniDFlow



Figure 6: Qualitative comparison of compositional text-to-image generation and editing. Prompts require precise grounding of attributes and spatial relations (red text). UniDFlow consistently adheres to these constraints while maintaining realistic structure and visual fidelity, outperforming prior unified baselines in fine-grained prompt alignment. More results can be found in Appendix F.

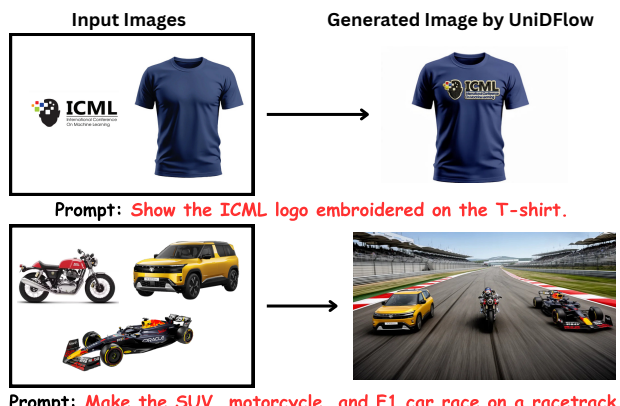


Figure 7: Subject-driven image generation with attribute editing and multi-object composition.

synthesizes a coherent output while preserving fine-grained visual details from the references. This behavior emerges from its unified multimodal optimization, which enables joint reasoning over object identity, attributes, and spatial relations.

4.3. Text-to-Image Editing

Table 3 summarizes the image editing performance of UniDFlow on IMGEDIT BENCH [71], EMU-EDIT [49], and GEDIT-BENCH-EN [33]. On EMU-EDIT, UniDFlow outperforms EMMA and Mammoth-Moda2 by approximately +3.5% and +4.1%, respectively, indicating stronger semantic alignment

Model	IMGEDIT				EMU-EDIT			GEDIT-BENCH-EN		
	Add ↑	Extract ↑	Remove↑	Overall ↑	CLIP-I ↑	CLIP-Out ↑	DINO ↑	SC ↑	PQ ↑	Overall ↑
FLUX.1 Kontext-Pro [28]	4.25	2.35	3.57	4.00	0.88	-	0.808	7.77	7.12	6.95
Bagel [14]	3.56	1.70	2.62	3.20	0.839	0.307	0.753	7.36	6.83	6.52
UniWorld-v1 [30]	3.82	2.27	3.24	3.26	-	-	-	4.93	7.43	4.85
OmniGen2 [65]	3.57	1.77	3.20	3.44	0.876	0.309	0.822	7.16	6.77	6.41
Emma [24]	4.52	3.54	4.21	4.01	0.911	0.311	0.834	7.33	7.54	6.52
MammothModa2 [48]	4.57	3.38	3.34	4.06	0.891	0.322	0.844	7.77	7.32	6.82
UniDFlow	4.66	4.01	4.24	4.24	0.921	0.362	0.862	8.01	7.82	7.12

Table 3: Text-to-image editing results. IMGEDIT metric is category-wise scores, while EMU-EDIT CLIP-I/DINO is used for source consistency and CLIP-Out for caption alignment. GEDIT-BENCH-EN evaluates SC (instruction following) and PQ (perceptual quality).

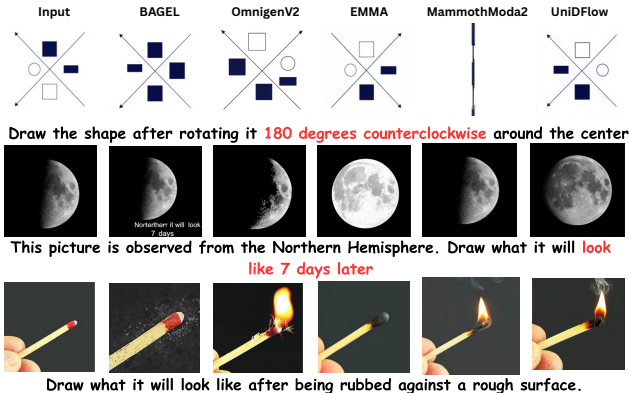


Figure 8: Reasoning-driven image editing, highlighting temporal, geometric, and physical transformations handled by UniDFlow.

between the input image, editing instruction, and edited output. On GEDIT-BENCH-EN, which emphasizes perceptual quality and instruction satisfaction, UniDFlow improves the averaged score by +3.7% over EMMA and +2.9% over MammothModa2.

Further, on IMAGEEDIT BENCH, which evaluates diverse editing scenarios including object manipulation, background changes, style transfer, and hybrid edits, UniDFlow achieves an overall score of 4.24, surpassing EMMA (4.01) and MammothModa2 (4.06) by +5.7% and +4.4%, respectively. Notably, the largest gains are observed in Extract and Remove operations, demonstrating more precise target isolation and reduced collateral degradation. These improvements are driven by reference-based preference alignment, which encourages UniDFlow to select higher-quality edits that better satisfy user intent.

Editing with reasoning. Fig. 8 compares models on editing tasks requiring temporal, geometric, and physical reasoning. UniDFlow generates outputs that better reflect the intended transformations while preserving object identity, benefiting from the strong reasoning priors inherited from the pretrained VLM backbone. Fig. 6 (bottom two rows) presents additional qualitative examples, where UniDFlow produces both accurate, large-scale semantic edits (e.g., style transfer) and fine-grained object-level modifications, exhibiting strong instruction fidelity and precise edit localization.

4.4. Ablations

Table 4 presents a comprehensive ablation study analyzing the key design choices of UniDFlow.

Model sizes. Performance improves consistently as model size increases across all benchmarks. Larger backbones provide stronger multimodal priors and improved capacity for modeling long-range dependencies, which benefits both reasoning and diffusion-based generation. Notably, even the 4B model achieves competitive performance, validating the parameter-efficient design of UniDFlow.

Visual tokenizer. UniDFlow uses PyraTok [54], which performs text-guided multi-scale quantization, enabling coarse-to-fine visual representations aligned with language. In contrast, 3D-MBQ-VAE [53] and MAGVIT-v2 [72] use single-scale, visually trained tokenizers, limiting hierarchical modeling and text alignment. SweetTok [56] incorporates text seman-

	EVAL	VLM	GEN	EVAL	DPG	BENCH	IMG	EDIT
UniDFlow	82.85	0.95	91.91	4.24				
1. Model Size Ablation								
Qwen3-0.6B	79.48	0.93	88.32	4.19				
Qwen3-4B	82.85	0.95	91.91	4.24				
Qwen3-8B	84.02	0.96	92.56	4.26				
Qwen3-14B	89.24	0.98	95.44	4.63				
2. Visual tokenizer								
3D-MBQ-VAE	81.27	0.92	91.43	4.19				
MAGVIT-v2	81.19	0.91	90.34	4.16				
SweetTok	80.76	0.92	90.44	4.12				
3. Architectural Ablations								
w/o LoRA _{text}	80.11	0.92	89.33	4.01				
w/o LoRA _{img}	81.23	0.93	90.05	4.08				
w/o MoRA	80.67	0.93	89.88	4.11				
Single LoRA (Und+Gen)	79.92	0.90	89.12	4.08				
4. Loss Function Ablations								
w/o $\mathcal{L}_{v\text{Ref-DPO}}$	80.45	0.91	88.44	4.09				
w/o $\mathcal{L}_{t\text{Ref-DPO}}$	79.45	0.91	90.32	4.18				
w/o $\mathcal{L}_{m\text{Ref-DPO}}$	77.34	0.86	86.23	4.05				
w/o Reflection	81.23	0.89	87.57	4.14				
5. Stage3-Alignment Training								
DPO	80.12	0.92	88.82	4.14				
uni-GRPO	80.88	0.93	90.07	4.18				

Table 4: Ablations on key UniDFlow components.

tics but lacks multi-scale quantization, reducing its ability to capture coarse-to-fine structure.

Components. Removing either understanding-specific or generation-specific LoRA adapters leads to noticeable degradation, confirming that separating task-specific adaptations is critical to avoid objective interference. Performance drops further when the router is removed, indicating that dynamic composition of adapters is necessary for balancing understanding and generation. Using a single shared LoRA fails entirely, demonstrating that naive parameter sharing causes severe entanglement between tasks.

Losses. Removing visual or text alignment losses degrades performance on corresponding benchmarks. Excluding reflection-based preference learning reduces editing and faithfulness metrics, showing that reasoning behind generation helps in precise instruction following and multimodal editing (refer to Appendix F for visual results).

Alignment Training. We align UniDFlow with DPO [43], uni-GRPO [70], and our mRef-DPO. Vanilla DPO can hurt when text–image tokens are weakly aligned, yielding noisy preference signals that degrade reasoning-grounded generation and edits. Uni-GRPO gives small gains but its group normaliza-

tion is unstable (especially on short prompts), reducing fine-grained edit reliability. mRef-DPO performs best by using modality-aware preference learning to stabilize cross-modal credit assignment between textual reasoning and diffusion steps, improving alignment and edit precision across metrics.

5. Conclusion

We introduce UniDFlow, a unified vision–language diffusion model that performs understanding, text-to-image generation, and instruction-guided editing within a single discrete flow-matching framework. We further propose *mRef-DPO*, a reference-anchored multimodal preference objective that jointly aligns text and image outputs against a frozen reference policy, improving faithfulness and controllability. Extensive results across six benchmarks show consistent gains, underscoring modality-aware preference alignment as critical for robust reasoning-grounded generation and precise visual edits.

Impact Statement

This work presents a unified multimodal generative system that combines high-level understanding with high-fidelity visual generation. Such systems can enhance accessibility, creativity, and productivity by enabling natural multimodal interaction, supporting educational and design workflows, and improving human–computer interfaces. Our parameter-efficient training approach can also reduce computational cost compared to large-scale end-to-end retraining, potentially lowering environmental impact.

At the same time, improved generation and editing capabilities introduce risks. High-quality multimodal synthesis can be misused for deceptive media manipulation, and precise editing may enable subtle alterations that are difficult to detect. Biases in pretrained vision–language backbones may propagate into generated outputs, leading to stereotypical or harmful representations. Our reference-based multimodal preference alignment aims to improve faithfulness and controllability by learning relative preferences under shared conditioning. This may help reduce spu-

rious correlations and limit amplification of dataset-specific artifacts when preference data is balanced. However, alignment quality depends on the diversity and representativeness of supervision signals, and misuse risks remain. Responsible deployment should therefore include safeguards such as content moderation, bias evaluation, and transparency mechanisms (e.g., watermarking or provenance tracking).

References

[1] Jean-Baptiste Alayrac, Jeff Donahue, Pauline Luc, Antoine Miech, Iain Barr, Yana Hasson, Karel Lenc, Arthur Mensch, Katherine Milligan, Malcolm Reynolds, et al. Flamingo: a visual language model for few-shot learning. *Advances in Neural Information Processing Systems (NeurIPS)*, 2022.

[2] Jacob Austin, Daniel D Johnson, Jonathan Ho, Daniel Tarlow, and Rianne Van Den Berg. Structured denoising diffusion models in discrete state-spaces. *Advances in Neural Information Processing Systems (NeurIPS)*, 2021.

[3] Jinze Bai, Shuai Bai, Yunfei Chu, Zeyu Cui, Kai Dang, Xiaodong Deng, Yang Fan, Wenbin Ge, Yu Han, Fei Huang, et al. Qwen technical report. *arXiv preprint arXiv:2309.16609*, 2023.

[4] Shuai Bai, Yunfei Chu, Jinze Ding, Kai Du, Xuancheng Fan, Xingzhou Fu, Wenbin Gan, Rui Ge, Zejun Han, Guohao Huang, et al. Qwen2.5-vl technical report. *arXiv preprint arXiv:2502.13923*, 2025.

[5] Shuai Bai, Yunfei Chu, Jinze Ding, et al. Qwen3-vl technical report. *arXiv preprint arXiv:2511.21631*, 2025.

[6] James Betker, Gabriel Goh, Li Jing, Tim Brooks, Jianfeng Wang, Linjie Li, Long Ouyang, Jun-tang Zhuang, Joyce Lee, Yufei Guo, et al. Improving image generation with better captions. *Computer Science. https://cdn. openai. com/papers/dall-e-3. pdf*, 2023.

[7] Umberto Borso, Davide Paglieri, Jude Wells, and Tim Rocktäschel. Preference-based align-
ment of discrete diffusion models. In *ICLR 2025 Workshop on Bidirectional Human-AI Alignment*, 2025.

[8] Huiwen Chang, Han Zhang, Lu Jiang, Ce Liu, and William T Freeman. Maskgit: Masked generative image transformer. In *IEEE Conference on Computer Vision and Pattern Recognition (CVPR)*, 2022.

[9] Junsong Chen, Jincheng Yu, Chongjian Ge, Lewei Yao, Enze Xie, Yue Wu, Zhongdao Wang, James Kwok, Ping Luo, Huchuan Lu, et al. Pixart-alpha: Fast training of diffusion transformer for photorealistic text-to-image synthesis. In *International Conference on Learning Representations (ICLR)*, 2024.

[10] Xiaokang Chen et al. Janus-pro: Unified multimodal understanding and generation with data and model scaling. *arXiv preprint arXiv:2501.12921*, 2025.

[11] Zhe Chen, Jiannan Wu, Wenhui Wang, Weijie Su, Guo Chen, Sen Xing, Muyan Zhong, Qianglong Zhang, Xizhou Zhu, Lewei Lu, et al. Internvl: Scaling up vision foundation models and aligning for generic visual-linguistic tasks. In *IEEE Conference on Computer Vision and Pattern Recognition (CVPR)*, 2024.

[12] Zhihong Chen, Xuehai Bai, Yang Shi, Chaoyou Fu, Huanyu Zhang, Haotian Wang, Xiaoyan Sun, Zhang Zhang, Liang Wang, Yuanxing Zhang, Pengfei Wan, and Yi-Fan Zhang. Openpft-4o-image: A comprehensive dataset for advanced image generation and editing. *arXiv preprint arXiv:2509.24900*, 2025.

[13] Xiaoliang Dai, Ji Hou, Chih-Yao Ma, Sam Tsai, Jialiang Wang, Rui Wang, Peizhao Zhang, Simon Vandenhende, Xiaofang Wang, Abhimanyu Dubey, et al. Emu: Enhancing image generation models using photogenic needles in a haystack. *arXiv preprint arXiv:2309.15807*, 2023.

[14] Chaorui Deng, Deyao Zhu, Kunchang Li, Chen-hui Gou, Feng Li, Zeyu Wang, Shu Zhong, Wei-

hao Yu, Xiaonan Nie, Ziang Song, et al. Emerging properties in unified multimodal pretraining. *arXiv preprint arXiv:2505.14683*, 2025.

[15] Patrick Esser, Sumith Kulal, Andreas Blattmann, Rahim Entezari, Jonas Müller, Harry Saini, Yam Levi, Dominik Lorenz, Axel Sauer, Frederic Boesel, et al. Scaling rectified flow transformers for high-resolution image synthesis. In *International Conference on Machine Learning (ICML)*, 2024.

[16] Chenfei Wu et al. Qwen-image technical report, 2025.

[17] Chaoyou Fu, Peixian Chen, Yunhang Shen, Yulei Qin, Mengdan Zhang, Xu Lin, Jinrui Yang, Xiawu Zheng, Ke Li, Xing Sun, et al. Mme: A comprehensive evaluation benchmark for multimodal large language models. *Advances in Neural Information Processing Systems (NeurIPS)*, 2023.

[18] Ling Fu, Zhebin Kuang, Jiajun Song, Mingxin Huang, Biao Yang, Yuzhe Li, Linghao Zhu, Qidi Luo, Xinyu Wang, Hao Lu, et al. Ocr-bench v2: An improved benchmark for evaluating large multimodal models on visual text localization and reasoning. *arXiv preprint arXiv:2501.00321*, 2024.

[19] Itai Gat, Tal Remez, Neta Shaul, Felix Kreuk, Ricky TQ Chen, Gabriel Synnaeve, Yossi Adi, and Yaron Lipman. Discrete flow matching. *Advances in Neural Information Processing Systems (NeurIPS)*, 2024.

[20] Michal Geyer, Omer Bar-Tal, Shai Bagon, and Tali Dekel. Tokenflow: Consistent diffusion features for consistent video editing. In *International Conference on Learning Representations (ICLR)*, 2023.

[21] Dhruba Ghosh, Hannaneh Hajishirzi, and Ludwig Schmidt. Geneval: An object-focused framework for evaluating text-to-image alignment. *Advances in Neural Information Processing Systems (NeurIPS)*, 2023.

[22] Ian J Goodfellow, Jean Pouget-Abadie, Mehdi Mirza, Bing Xu, David Warde-Farley, Sherjil Ozair, Aaron Courville, and Yoshua Bengio. Generative adversarial nets. *Advances in Neural Information Processing Systems (NeurIPS)*, 2014.

[23] Shuyang Gu, Dong Chen, Jianmin Bao, Fang Wen, Bo Zhang, Dongdong Chen, Lu Yuan, and Baining Guo. Vector quantized diffusion model for text-to-image synthesis. In *IEEE Conference on Computer Vision and Pattern Recognition (CVPR)*, 2022.

[24] Xin He, Longhui Wei, Jianbo Ouyang, Lingxi Xie, and Qi Tian. Emma: Efficient multi-modal understanding, generation, and editing with a unified architecture. *arXiv preprint arXiv:2512.04810*, 2025.

[25] Jonathan Ho, Ajay Jain, and Pieter Abbeel. Denoising diffusion probabilistic models. *Advances in Neural Information Processing Systems (NeurIPS)*, 2020.

[26] Xiwei Hu, Rui Wang, Yixiao Fang, Bin Fu, Pei Cheng, and Gang Yu. Ella: Equip diffusion models with llm for enhanced semantic alignment. *arXiv preprint arXiv:2403.05135*, 2024.

[27] Jackyhate. text-to-image-2m dataset (hugging face: jackyhate/text-to-image-2m), 2024.

[28] Black Forest Labs, Stephen Batifol, Andreas Blattmann, Frederic Boesel, Saksham Consul, Cyril Diagne, Tim Dockhorn, Jack English, et al. Flux.1 kontext: Flow matching for in-context image generation and editing in latent space. *arXiv preprint arXiv:2506.15742*, 2025.

[29] Junnan Li, Dongxu Li, Silvio Savarese, and Steven Hoi. Blip-2: Bootstrapping language-image pre-training with frozen image encoders and large language models. In *International Conference on Machine Learning (ICML)*, 2023.

[30] Bin Lin, Zongjian Li, Xinhua Cheng, Yuwei Niu, Yang Ye, Xianyi He, Shanghai Yuan,

Wangbo Yu, Shaodong Wang, Yunyang Ge, Yatian Pang, and Li Yuan. Uniworld-v1: High-resolution semantic encoders for unified visual understanding and generation. *arXiv preprint arXiv:2506.03147*, 2025.

[31] Aixin Liu, Bei Feng, Bing Xue, Bingxuan Wang, Bochao Wu, Chengda Lu, Chenggang Zhao, Chengqi Deng, Chenyu Zhang, Chong Ruan, et al. Deepseek-v3 technical report. *arXiv preprint arXiv:2412.19437*, 2024.

[32] Haotian Liu, Chunyuan Li, Qingyang Wu, and Yong Jae Lee. Visual instruction tuning. *Advances in Neural Information Processing Systems (NeurIPS)*, 2023.

[33] Shiyu Liu, Yucheng Han, Peng Xing, Fukun Yin, Rui Wang, Wei Cheng, Jiaqi Liao, Yingming Wang, Honghao Fu, Chunrui Han, et al. Step1x-edit: A practical framework for general image editing. *arXiv preprint arXiv:2504.17761*, 2025.

[34] Yangzhou Liu, Yue Cao, Zhangwei Gao, Weiyun Wang, Zhe Chen, Wenhui Wang, Hao Tian, Lewei Lu, Xizhou Zhu, Tong Lu, Yu Qiao, and Jifeng Dai. Mminstruct: A high-quality multi-modal instruction tuning dataset with extensive diversity. *Science China Information Sciences*, 2024.

[35] Yuanzhan Liu, Haodong Duan, Yuanhan Zhang, Bo Li, Songyang Zhang, Wangbo Zhao, Yike Yuan, Jiaqi Wang, Conghui He, Ziwei Liu, et al. Mmbench: Is your multi-modal model an all-around player? In *European Conference on Computer Vision (ECCV)*, 2024.

[36] Pan Lu, Hritik Bansal, Tony Xia, Jiacheng Liu, Chunyue Li, Hannaneh Hajishirzi, Hao Cheng, Kai-Wei Chang, Michel Galley, and Jianfeng Gao. Mathvista: Evaluating mathematical reasoning of foundation models in visual contexts. In *International Conference on Learning Representations (ICLR)*, 2024.

[37] Yihong Luo, Tianyang Hu, and Jing Tang. Reinforcing diffusion models by direct group preference optimization. *arXiv preprint arXiv:2510.08425*, 2025.

[38] Alex Nichol, Prafulla Dhariwal, Aditya Ramesh, Pranav Shyam, Pamela Mishkin, Bob McGrew, Ilya Sutskever, and Mark Chen. Glide: Towards photorealistic image generation and editing with text-guided diffusion models. In *International Conference on Machine Learning (ICML)*, 2021.

[39] OpenAI. Chatgpt, 2022. URL <https://chat.openai.com/>. Large language model, accessed 2 Jan 2026.

[40] OpenAI. Gpt-4o mini: Advancing cost-efficient intelligence, 2024.

[41] Dustin Podell, Zion English, Kyle Lacey, Andreas Blattmann, Tim Dockhorn, Jonas Müller, Joe Penna, and Robin Rombach. Sdxl: Improving latent diffusion models for high-resolution image synthesis. In *International Conference on Learning Representations (ICLR)*, 2023.

[42] Yusu Qian, Eli Bocek-Rivele, Liangchen Song, Jialing Tong, Yinfei Yang, Jiasen Lu, Wenze Hu, and Zhe Gan. Pico-banana-400k: A large-scale dataset for text-guided image editing. *arXiv preprint arXiv:2510.19808*, 2025.

[43] Rafael Rafailov, Archit Sharma, Eric Mitchell, Christopher D Manning, Stefano Ermon, and Chelsea Finn. Direct preference optimization: Your language model is secretly a reward model. *Advances in Neural Information Processing Systems (NeurIPS)*, 2023.

[44] Aditya Ramesh, Mikhail Pavlov, Gabriel Goh, Scott Gray, Chelsea Voss, Alec Radford, Mark Chen, and Ilya Sutskever. Zero-shot text-to-image generation. In *International Conference on Machine Learning (ICML)*, 2021.

[45] Robin Rombach, Andreas Blattmann, Dominik Lorenz, Patrick Esser, and Björn Ommer. High-resolution image synthesis with latent diffusion models. In *IEEE Conference on Computer Vision and Pattern Recognition (CVPR)*, 2022.

[46] Chitwan Saharia, William Chan, Saurabh Saxena, Lala Li, Jay Whang, Emily L Denton, Kamyar Ghasemipour, Raphael Gontijo Lopes, Burcu Karagol Ayan, Tim Salimans, et al. Photorealistic text-to-image diffusion models with deep language understanding. *Advances in Neural Information Processing Systems (NeurIPS)*, 2022.

[47] Christoph Schuhmann, Romain Beaumont, Richard Vencu, Cade Gordon, Ross Wightman, Mehdi Cherti, Theo Coombes, Aarush Katta, Clayton Mullis, Mitchell Wortsman, Patrick Schramowski, Srivatsa Kundurthy, Katherine Crowson, Ludwig Schmidt, Robert Kaczmarczyk, and Jenia Jitsev. Laion-5b: An open large-scale dataset for training next generation image-text models. *Advances in Neural Information Processing Systems (NeurIPS)*, 2022.

[48] Tao Shen, Xin Wan, Taicai Chen, Rui Zhang, Junwen Pan, Dawei Lu, Fanding Lei, Zhilin Lu, Yunfei Yang, Chen Cheng, et al. Mammothmoda2: A unified ar-diffusion framework for multimodal understanding and generation. *arXiv preprint arXiv:2511.18262*, 2025.

[49] Shelly Sheynin, Adam Polyak, Uriel Singer, Yuval Kirstain, Amit Zohar, Oron Ashual, Devi Parikh, and Yaniv Taigman. Emu edit: Precise image editing via recognition and generation tasks. In *IEEE Conference on Computer Vision and Pattern Recognition (CVPR)*, 2024.

[50] Qingyu Shi, Jinbin Bai, Zhuoran Zhao, Wenhao Chai, Kaidong Yu, Jianzong Wu, Shuangyong Song, Yunhai Tong, Xiangtai Li, Xuelong Li, et al. Muddit: Liberating generation beyond text-to-image with a unified discrete diffusion model. *arXiv preprint arXiv:2505.23606*, 2025.

[51] Keqiang Sun, Junting Pan, Yuying Ge, Hao Li, Haodong Duan, Xiaoshi Wu, Renrui Zhang, Ao-jun Zhou, Zipeng Qin, Yi Wang, Jifeng Dai, Yu Qiao, Limin Wang, and Hongsheng Li. Journeydb: A benchmark for generative image understanding. *Advances in Neural Information Processing Systems (NeurIPS)*, 2023.

[52] Quan Sun, Yufeng Cui, Xiaosong Zhang, Fan Zhang, Qiying Yu, Yueze Wang, Yongming Rao, Jingjing Liu, Tiejun Huang, and Xinlong Wang. Generative multimodal models are in-context learners. In *IEEE Conference on Computer Vision and Pattern Recognition (CVPR)*, 2024.

[53] Onkar Susladkar, Jishu Sen Gupta, Chirag Sehgal, Sparsh Mittal, and Rekha Singhal. Motionaura: Generating high-quality and motion consistent videos using discrete diffusion. In *International Conference on Learning Representations (ICLR)*, 2024.

[54] Onkar Susladkar, Tushar Prakash, Adheesh Juvvekar, Kiet A Nguyen, Dong-Hwan Jang, Inderjit S Dhillon, and Ismini Lourentzou. Pyratok: Language-aligned pyramidal tokenizer for video understanding and generation. *arXiv preprint arXiv:2601.16210*, 2026.

[55] Alexander Swerdlow, Mihir Prabhudesai, Siddharth Gandhi, Deepak Pathak, and Katerina Fragkiadaki. Unified multimodal discrete diffusion. *arXiv preprint arXiv:2503.20853*, 2025.

[56] Zhentao Tan, Ben Xue, Jian Jia, Junhao Wang, Wencai Ye, Shaoyun Shi, Mingjie Sun, Wenjin Wu, Quan Chen, and Peng Jiang. Sweettok: Semantic-aware spatial-temporal tokenizer for compact video discretization. In *International Conference on Computer Vision (ICCV)*, 2025.

[57] Chameleon Team. Chameleon: Mixed-modal early-fusion foundation models. *arXiv preprint arXiv:2405.09818*, 2024.

[58] Gemini Team, Rohan Anil, Sebastian Borgeaud, Jean-Baptiste Alayrac, Jiahui Yu, Radu Soricut, Johan Schalkwyk, Andrew M Dai, Anja Hauth, Katie Millican, et al. Gemini: a family of highly capable multimodal models, 2023.

[59] Shengbang Tong, Zhuang Liu, Yuxian Zhai, Yi Ma, Yann LeCun, and Saining Xie. Eyes wide shut? exploring the visual shortcomings of multimodal llms. In *IEEE Conference on Computer Vision and Pattern Recognition (CVPR)*, 2024.

[60] Hugo Touvron, Thibaut Lavril, Gautier Izacard, Xavier Martinet, Marie-Anne Lachaux, Timothée Lacroix, Baptiste Rozière, Naman Goyal, Eric Hambro, Faisal Azhar, et al. Llama: Open and efficient foundation language models. *arXiv preprint arXiv:2302.13971*, 2023.

[61] Ashish Vaswani, Noam Shazeer, Niki Parmar, Jakob Uszkoreit, Llion Jones, Aidan N Gomez, Łukasz Kaiser, and Illia Polosukhin. Attention is all you need. *Advances in Neural Information Processing Systems (NeurIPS)*, 2017.

[62] Bram Wallace, Meihua Dang, Rafael Rafailov, Linqi Zhou, Aaron Lou, Senthil Purushwalkam, Stefano Ermon, Caiming Xiong, Shafiq Joty, and Nikhil Naik. Diffusion model alignment using direct preference optimization. In *IEEE Conference on Computer Vision and Pattern Recognition (CVPR)*, 2024.

[63] Xin Wang, Yuwei Zhou, Bin Huang, Hong Chen, and Wenwu Zhu. Multi-modal generative ai: Multi-modal llms, diffusions and the unification. *IEEE Transactions on Circuits and Systems for Video Technology*, 2024.

[64] WINDop. Opengpt-4o-image dataset (hugging face: Windop/opengpt-4o-image), 2025. URL <https://huggingface.co/datasets/WINDop/OpenGPT-4o-Image>.

[65] Chenyuan Wu, Pengfei Zheng, Ruiran Yan, Shitao Xiao, Xin Luo, Yueze Wang, Wanli Li, Xiyan Jiang, Yexin Liu, Junjie Zhou, et al. Omnigen2: Exploration to advanced multimodal generation. *arXiv preprint arXiv:2506.18871*, 2025.

[66] Yixiao Wu, Haotian Lin, et al. Vila-u: A unified foundation model integrating visual understanding and generation. *arXiv preprint arXiv:2409.04429*, 2024.

[67] Zhiyu Wu, Xiaokang Liu, Huaiyuan Lin, et al. Deepseek-vl2: Mixture-of-experts vision-language models for advanced multimodal understanding. *arXiv preprint arXiv:2412.10302*, 2024.

[68] Jinheng Xie, Weijia Mao, Zechen Bai, David Junhao Zhang, Weihao Wang, Kevin Qinghong Lin, Yuchao Gu, Zhijie Chen, Zhenheng Yang, and Mike Zheng Shou. Show-o: One single transformer to unify multimodal understanding and generation. In *International Conference on Learning Representations (ICLR)*, 2024.

[69] Le Xue, Manli Shu, Evan Shelhamer, Haotian He, Wang Wild, Ran Xu, et al. xgen-mm (blip-3): A family of open large multimodal models. *arXiv preprint arXiv:2408.08872*, 2024.

[70] Ling Yang, Ye Tian, Bowen Li, Xinchen Zhang, Ke Shen, Yunhai Tong, and Mengdi Wang. Mmada: Multimodal large diffusion language models. *arXiv preprint arXiv:2505.15809*, 2025.

[71] Yang Ye, Xianyi He, Zongjian Li, Bin Lin, Shanghai Yuan, Zhiyuan Yan, Bohan Hou, and Li Yuan. Imgedit: A unified image editing dataset and benchmark. *arXiv preprint arXiv:2505.20275*, 2025.

[72] Lijun Yu, Jose Lezama, Nitesh Bharadwaj Gundavarapu, Luca Versari, Kihyuk Sohn, David Minnen, Yong Cheng, Agrim Gupta, Xiuye Gu, Alexander G Hauptmann, et al. Language model beats diffusion-tokenizer is key to visual generation. In *International Conference on Learning Representations (ICLR)*, 2024.

[73] Qifan Yu, Wei Chow, Zhongqi Yue, Kaihang Pan, Yang Wu, Xiaoyang Wan, Juncheng Li, Siliang Tang, Hanwang Zhang, and Yueting Zhuang. Anyedit: Mastering unified high-quality image editing for any idea. In *IEEE Conference on Computer Vision and Pattern Recognition (CVPR)*, 2024.

[74] Weihao Yu, Zhengyuan Yang, Linjie Li, Jianfeng Wang, Kevin Lin, Zicheng Liu, Xinchao Wang, and Lijuan Wang. Mm-vet: Evaluating large multimodal models for integrated capabilities. In *International Conference on Machine Learning (ICML)*, 2024.

- [75] Xiang Yue, Yuansheng Ni, Kai Zhang, Tianyu Zheng, Ruoqi Liu, Ge Zhang, Samuel Stevens, Dongfu Jiang, Weiming Ren, Yuxuan Sun, et al. Mmmu: A massive multi-discipline multimodal understanding and reasoning benchmark for expert agi. In *IEEE Conference on Computer Vision and Pattern Recognition (CVPR)*, 2024.
- [76] Xiaohua Zhai, Basil Mustafa, Alexander Kolesnikov, and Lucas Beyer. Sigmoid loss for language image pre-training. In *IEEE Conference on Computer Vision and Pattern Recognition (CVPR)*, 2023.
- [77] Lvmin Zhang, Anyi Rao, and Maneesh Agrawala. Adding conditional control to text-to-image diffusion models. In *IEEE Conference on Computer Vision and Pattern Recognition (CVPR)*, 2023.
- [78] Yu Zhong, Tianwei Lin, Ruike Zhu, Yuqian Yuan, Haoyu Zheng, Liang Liang, Wenqiao Zhang, Feifei Shao, Haoyuan Li, Wanggui He, et al. Unified personalized understanding, generating and editing. *arXiv preprint arXiv:2601.06965*, 2026.
- [79] Huaisheng Zhu, Teng Xiao, and Vasant G Honavar. Dspo: Direct score preference optimization for diffusion model alignment. In *International Conference on Learning Representations (ICLR)*, 2025.

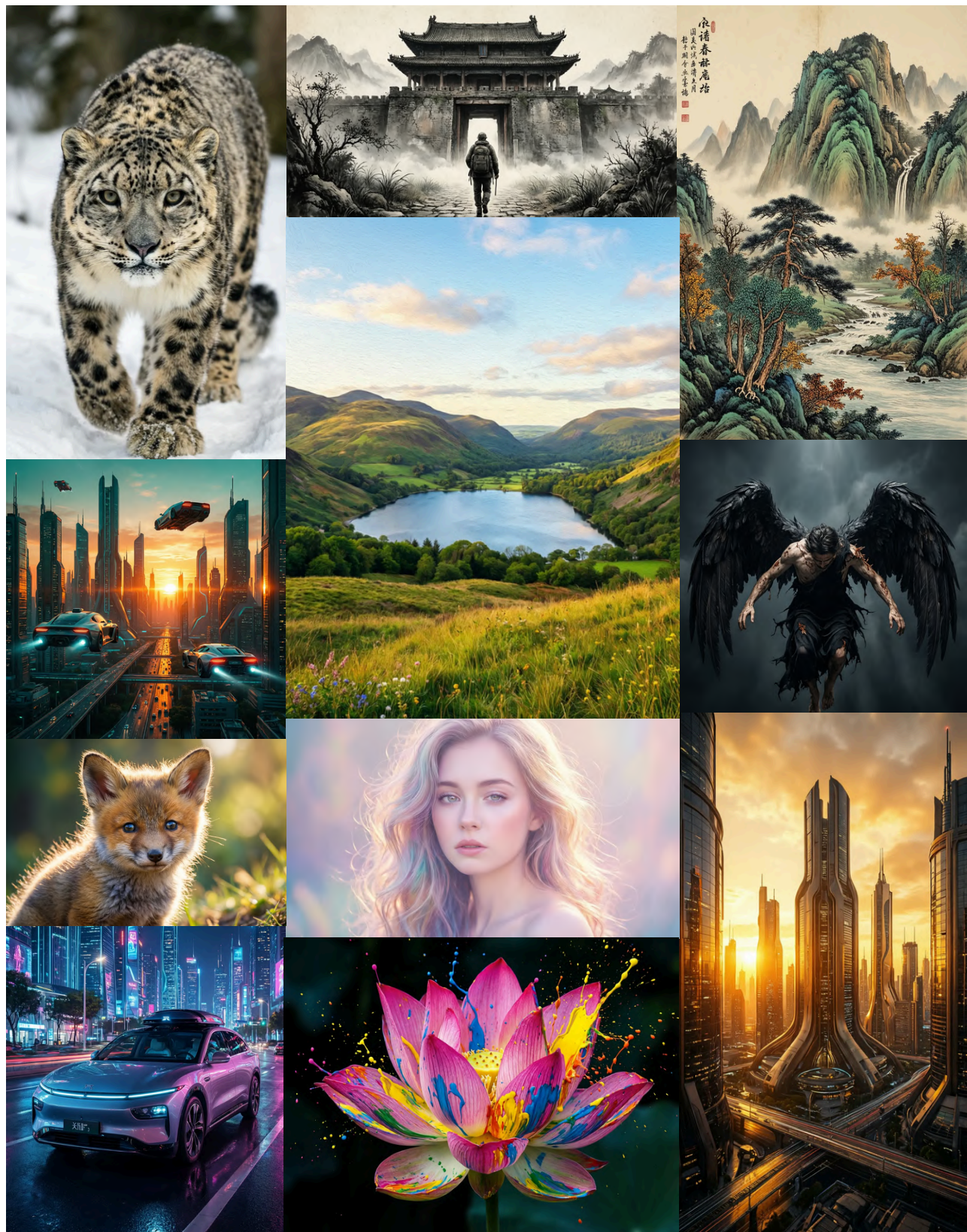


Figure 9: Image Generation with UniDFlow

Hyperparam Setting	Stage 1	Stage 2	Stage 3
GPUs	32xA100 (80GB)	32xH100 (80GB)	48xH100 (80GB)
Batch / GPU	8	6	4
Optimizer	AdamW	AdamW	AdamW
Init LR	1×10^{-5}	5×10^{-5}	2×10^{-5}
LR schedule	Cosine	Linear	Cosine
Warmup steps	200	1000	1200
Train steps	10K	25K	30K
Grad accumulation	6	4	4
Max grad norm	2.0	1.0	2.0
Weight decay	0	1×10^{-2}	1×10^{-3}
Diffusion steps	40	50	50
Classifier-free guidance	8	8	12
Resolution	224-1024	256/512/768/1024	224-1280
Aspect ratios	1:1, 4:3, 3:4	1:1, 16:9, 9:16	1:1, 4:3, 3:4, 16:9, 9:16
Max seq length	2048	2048	4096
Precision	BF16	BF16	BF16
GPU-Hours	256	320	528

Table 5: Training setup by stage. Stages 1–3 correspond to instruction tuning, visual generation, and joint understanding/alignment.

A. Implementation Details

We employ a three-stage training pipeline (Table 5) that progressively builds (i) visual instruction-following capability, (ii) high-fidelity visual generation, and (iii) joint multimodal understanding and alignment. Across all stages, we use AdamW optimization with mixed-precision training and gradient clipping to stabilize training at scale.

Stage 1: Text Alignment We first perform supervised fine-tuning to teach the model to follow visual instructions and ground text responses in images. To improve robustness to real-world inputs, we train with variable aspect ratios and variable image resolutions, enabling the model to generalize across diverse image formats. The learning-rate schedule uses a warmup phase followed by cosine annealing for stable convergence.

Stage II: Visual Alignment Next, we train the model for visual generation using a diffusion-based objective. We train at multiple resolutions (with variable aspect ratios) to encourage both global structure and fine detail, and use a linear learning-rate schedule with a longer warmup to support stable optimization under the generative objective. Regularization is applied via weight decay to improve generalization.

Reference-Based Multimodal Preference Alignment Finally, we jointly optimize understanding and alignment, combining multimodal comprehension with aligned outputs. We expand the image

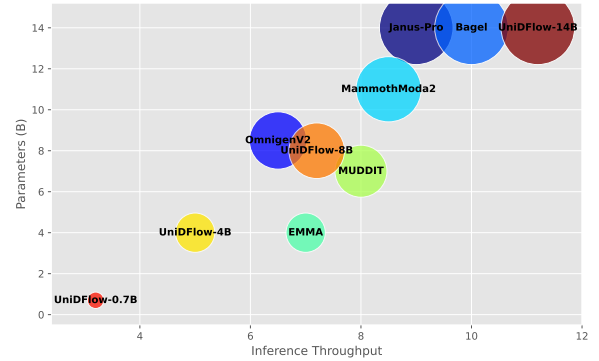


Figure 10: Inference throughput versus parameter count (in billions) for representative baselines and our model family. Higher throughput (right) is better, while fewer parameters (down) are more compact. resolution range further and increase the maximum sequence length to support longer-context reasoning over visual content. This stage uses a cosine-annealed schedule with warmup and moderate regularization, aiming to consolidate gains from the first two stages while maintaining training stability at scale.

Throughput-size trade-off. Figure 10 summarizes the empirical efficiency landscape by plotting inference throughput against model size for a set of representative systems (Janus-Pro [10], OmnigenV2 [65], Bagel [14], MammothModa2 [48], EMMA [24], and MUDDIT [50]) and our variants at 0.7B, 4B, 8B, and 14B parameters. Rather than exhibiting a strictly monotonic dependence on parameter count, the scatter shows substantial dispersion across independently implemented models, indicating that architectural choices and inference stacks materially affect end-to-end throughput beyond raw scale. In the large-model regime (~14B), UniDFlow-14B attains the highest throughput among the compared methods, outperforming other models of similar size (e.g., Bagel and Janus-Pro), suggesting improved runtime efficiency at scale. At intermediate sizes (~7–9B), UniDFlow-8B is competitive with contemporaneous baselines, while the smaller UniDFlow-0.7B and UniDFlow-4B provide lightweight operating points that prioritize compactness with correspondingly lower throughput.

B. Training Data

We employ a three-stage data curriculum that progressively transitions from supervised multimodal in-

St. Obj.	# Tok.		
1 SFT (MMInstruct)	1.0M	0.6T	
2 T2I (refined)	4.5M	1.2T	
3 Pref align.	3.5M	1.8T	
Total	3.6T		

Table 6: Stage-wise data (image+text tokens).

struction learning to large-scale image-text pretraining and finally preference-based alignment for unified understanding, generation, and editing. Table 6 provides a summary of the data used in training.

Token accounting. Throughout this work, the reported token counts include *both* text tokens and discretized/embedded image tokens as consumed by the multimodal sequence interface (*i.e.*, the effective sequence length seen by the transformer). We report aggregate tokens per stage.

Stage 1: Text Alignment. In Stage 1, we initialize instruction-following behavior using MMInstruct [34], a high-quality multimodal instruction tuning dataset spanning diverse domains and instruction types. We use approximately 1.0M image–prompt–answer examples (MMInstruct reports 973K instructions [34]) and train for $\approx 0.6T$ total (image+text) tokens.

Stage 2: Visual Alignment. Stage 2 focuses on *text-to-image generative pretraining* to improve prompt adherence, compositional generalization, and broad visual coverage. We sample a total of $\approx 4.5M$ images (with associated text prompts/captions) from three sources: (i) 1.5M from LAION-5B [47], (ii) 1.0M from JourneyDB [51], and (iii) 2.0M from the jackyhate/text-to-image-2M collection on Hugging Face [27]. We refine and normalize the paired text using a proprietary LLM-based caption/prompt rewriting pipeline to reduce noise and increase instruction clarity, and train for $\approx 1.2T$ total (image+text) tokens.

Stage III: Reference-Based Multimodal Preference Alignment. Stage 3 aligns the model to high-quality, instruction-faithful outputs in our unified data format for (a) multimodal understanding, (b) image generation, and (c) image editing. We curate $\approx 3.5M$ base tasks by aggregating: OpenGPT-4o-Image

($\sim 80K$) [12, 64], AnyEdit-derived edits ($\sim 3.0M$; AnyEdit reports 2.5M editing pairs) [73], and Pico-Banana-400K ($\sim 400K$) [42]. We then convert these tasks into a high-quality preference dataset via rejection-sampling style annotation using proprietary multimodal LLMs. For each edit instance, we generate and store (i) *reflection* traces with a positive:negative ratio of 3 : 6, and (ii) paired instruction/response candidates with positive:negative ratio 4 : 10 (stored as accepted vs. rejected candidates in our format). Stage 3 consumes $\approx 1.8T$ total tokens.

C. Extended Related Work

Diffusion for Visual Generation. Diffusion probabilistic models (DPMs) [25, 38, 46] surpass GANs [22] in stability and generation quality, but are computationally expensive due to pixel-space diffusion. Latent diffusion models (LDMs) [45] mitigate this cost by operating in a compressed latent space and achieve strong text-to-image performance [9, 41, 77]. However, continuous Gaussian diffusion is well-suited for images but less natural for discrete modalities such as text. Discrete diffusion [2] addresses this by using categorical corruption (*e.g.*, masking), motivating image generators that replace autoregressive decoding with parallel mask-and-predict refinement, improving both fidelity and latency [8, 23].

LLMs and VLMs for Understanding Large language models (LLMs) [31, 60] have achieved strong zero-shot reasoning and instruction-following by autoregressively generating tokens with decoder-only Transformers [61]. Inspired by their success, vision–language models (VLMs) [3, 4] extend LLMs to visual inputs by coupling a vision encoder (*e.g.*, SigLIP [76]) with a language model via lightweight projection layers, treating images as sequences of visual tokens. Models such as Qwen [5], LLaVA [32], BLIP-2 [29], and Flamingo [1] enable strong visual understanding (*e.g.*, captioning, VQA), but treat vision as read-only and rely on separate diffusion models for image generation.

Beyond likelihood training, preference alignment has been extended from LLMs to diffusion models using

Table 7: Evaluation of existing VLMs/MLLMs on English tasks of OCRBench v2 [18] public data. “Recognition”, “Referring”, “Spotting”, “Extraction”, “Parsing”, “Calculation”, “Understanding”, and “Reasoning” refer to text recognition, text referring, text spotting, relation extraction, element parsing, mathematical calculation, visual text understanding, and knowledge reasoning, respectively. Higher values indicate better performance.

Method	Recog.	Ref.	Spot.	Extr.	Pars.	Calc.	Und.	Reas.	Avg.
Qwen2.5-VL-7B [4]	68.8	25.7	1.2	80.2	30.4	38.2	73.2	56.2	46.7
InternVL3-14B [11]	67.3	36.9	11.2	89.0	38.4	38.4	79.2	60.5	52.6
GPT-4o [39]	61.2	26.7	0.0	77.5	36.3	43.4	71.1	55.5	46.5
GPT-4o-mini [40]	57.9	23.3	0.6	70.8	31.5	38.8	65.9	55.1	43.0
Gemini-pro [58]	61.2	39.5	13.5	79.3	39.2	47.7	75.5	59.3	51.9
Qwen3-VL-8B [5]	64.4	38.2	5.7	91.03	37.8	44.2	76.8	62.6	55.7
OmniGenV2 [65]	61.3	36.5	2.4	87.23	33.4	40.7	72.7	65.7	48.7
Begal [14]	65.8	37.1	3.3	90.45	38.5	41.3	75.2	66.4	52.2
Emma [24]	66.7	36.5	6.7	91.3	37.5	44.5	76.7	67.2	53.8
Muddit [50]	64.9	38.4	13.7	92.6	34.5	49.4	78.3	66.1	54.7
MammothModa2 [48]	68.2	39.5	11.4	92.2	39.1	50.2	80.2	68.1	56.1
UniDFlow-4B	69.9	41.2	12.9	94.1	42.2	53.4	83.1	70.8	58.4
UniDFlow-8B	72.2	43.8	14.9	95.0	45.7	55.1	85.9	73.5	60.7
UniDFlow-14B	76.7	47.1	16.5	96.9	48.4	58.1	88.7	77.1	63.8

DPO-style objectives [43]. Diffusion-DPO [62] directly fine-tunes text-to-image models on pairwise human judgments via a likelihood-based preference loss, while DSPO [79] instead aligns the diffusion score function in score space, staying closer to the original training objective. Subsequent variants such as DGPO [37] improve stability through group-wise preference optimization, and recent work further generalizes DPO-style alignment to discrete diffusion processes [7], bridging continuous and categorical diffusion frameworks.

Unified Models for Understanding and Generation Diffusion models and vision–language models excel at generation and semantic understanding, respectively, motivating unified architectures. To improve generation and editing, recent models add additional alignment stages. OmniGenV2 [65] employs multimodal reflection for self-correction, while MammothModa2 [48] applies reinforcement learning with scalar rewards (e.g., OCR and aesthetic scores). In contrast, UniDFlow introduces reference-based preference alignment across text and vision with reflection, enabling stable and faithful generation and editing.

D. Scene Text Reasoning and Recognition

Table 7 reports accuracy on eight visual reasoning subtasks, Recognition, Referring, Spotting, Extraction, Parsing, Calculation, Understanding, and Reasoning, together with their macro Average on OCRBenchV2 [18]. The compared systems include strong understanding-focused VLMs (e.g., Qwen2.5-VL [4], InternVL [11]), unified understanding–generation models (e.g., EMMA [24], BEGAL [14], Muddit [50], MammothModa2 [48]), and proprietary multimodal assistants (e.g., GPT-4o [39], Gemini-Pro [58]). Fig. 18 shows that robustness UniDFlow on complex understanding. This evaluation is particularly diagnostic because it separates perceptual grounding (Recognition/Spotting/Extraction), structured interpretation (Parsing/Calculation), and holistic inference (Understanding/Reasoning).

Across model scales, our unified model family consistently dominates the subtask profile, with performance improving monotonically from Ours-4B → Ours-8B → Ours-14B. Concretely, Ours-14B achieves the best overall Average = 63.8, improving over the strongest baseline (MammothModa2, 56.1) by +7.7

Model	Params	Single Obj	Two Obj	Counting	Colors	Position	Color Attr
DALL-E 3 [6]	–	0.96	0.87	0.47	0.83	0.43	0.45
SD3-Medium [15]	2B	0.99	0.94	0.72	0.89	0.33	0.60
Qwen-Image [16]	7B+20B	1.00	0.95	0.93	0.92	0.87	0.83
TokenFlow-XL [20]	14B	0.95	0.60	0.41	0.81	0.16	0.24
Janus-Pro-7B [10]	7B	0.99	0.89	0.59	0.90	0.79	0.66
Bagel [14]	7B+7B	0.98	0.95	0.84	0.95	0.78	0.77
OmniGen2/V2 [65]	3B+4B	0.95	0.93	0.64	0.81	0.73	0.74
MammothModa-2 [48]	8B+3B+2B	1.00	0.97	0.63	0.89	0.90	0.82
EMMA [24]	4B	1.00	0.99	0.87	0.98	0.86	0.87
MUDDIT [50]	7B	0.95	0.93	0.85	0.96	0.82	0.84
UniDFlow	4B	1.00	0.99	0.89	0.98	0.97	0.93

Table 8: Evaluation of text-to-image generation ability on GenEval benchmark.

Model	Params	Global	Entity	Attribute	Relation	Other
DALL-E 3 [6]	–	90.97	89.61	89.39	90.58	89.83
SD3-Medium [15]	2B	87.92	91.01	88.48	80.72	86.81
Qwen-Image [16]	7B + 20B	91.32	91.56	92.02	94.31	92.73
TokenFlow-XL [20]	14B	87.33	88.54	89.01	85.09	86.55
Janus-Pro-7B [10]	7B	86.91	88.95	89.43	90.02	89.48
Bagel [14]	7B + 7B	89.42	91.43	90.42	92.34	88.78
OmniGen2/V2 [65]	3B + 4B	–	–	86.43	91.23	–
MammothModa-2 [48]	8B + 3B + 2B	81.16	92.99	90.16	94.35	84.81
EMMA [24]	4B	91.24	91.71	90.59	92.23	90.02
MUDDIT [50]	7B	89.42	90.47	89.56	90.72	88.63
UniDFlow	4B	93.42	94.44	95.34	95.03	93.86

Table 9: Quantitative evaluations of the text-to-image generation capacity on DPG-Bench.

points. Gains are broad rather than concentrated in a single capability: relative to the best previous work in every column, Ours-14B improves Recognition (76.7; +7.9), Referring (47.1; +7.6), Spotting (16.5; +2.8), Extraction (96.9; +4.3), Parsing (48.4; +9.2), Calculation (58.1; +7.9), Understanding (88.7; +8.5), and Reasoning (77.1; +9.0). The largest deltas occur in Parsing and Reasoning, suggesting that the proposed approach strengthens compositional/structured visual reasoning beyond raw perception.

A second takeaway is that even the compact variant (Ours-4B) is competitive with or better than substantially larger baselines: it reaches 58.4 Avg., exceeding MammothModa2 (56.1) and MUDDIT (54.7) while also improving the hardest “reasoning-heavy” columns (Calc. = 53.4, Reas. = 70.8). This aligns with the paper’s core design choice: rather than en-

tangling understanding and generation in shared parameters, the method trains separate lightweight adapters for understanding vs. generation and combines them with a learned router, reducing objective interference and preserving specialization.

E. Full Quantitative Results on GenEval and DPGBench

The main paper reports the overall performance of UniDFlow on GenEval and DPGBench. Here, we provide the complete attribute-wise breakdown used by both benchmarks. Tables 8 and 9 show that UniDFlow achieves the best *global* score and consistently improves across fine-grained categories (e.g., entity, attribute, relation) as well as compositional criteria (single/two-object, counting, color, position, and color-attribute). These results indicate that the gains

are not driven by a single subset of prompts; instead, UniDFlow improves performance uniformly across evaluation dimensions, reflecting stronger text–image alignment and more reliable adherence to structured constraints.

F. Additional Results

Ablation on training tokens and LoRA rank. We study the effect of (i) the total number of pre-training tokens (image+text) and (ii) the LoRA rank used for adaptation. Figure 12 shows a consistent improvement as we scale the training budget from 0.5T to 3T tokens, yielding substantial gains across *TextGen*, *GenEval* [21], *DPGBench* [26], and *ImgEdit-Bench* [71]. We also ablate the LoRA rank and observe that increasing the rank from 8 to 32 produces the largest marginal improvement across all benchmarks, indicating that low ranks under-parameterize the adaptation. Beyond rank 32, performance improvements diminish and largely saturate up to rank 128, suggesting the adaptation becomes capacity-sufficient. Based on this accuracy-efficiency trade-off, we use a default LoRA rank of 64 in all experiments.

Ablation on Stage-III losses. Fig 14 presents qualitative examples for image editing without Stage-III alignment losses. Removing any single loss term degrades instruction-following and visual realism: in text-to-image generation, w/o variants show noticeable drift in composition and reduced coherence, while in image editing, they yield weaker target edits (e.g., less natural object replacement and less consistent candle ignition) and poorer photometric integration with the original scene. In contrast, UniDFlow produces the most faithful and visually consistent results across all three prompts, indicating that Stage-III losses are complementary and jointly necessary for robust alignment.

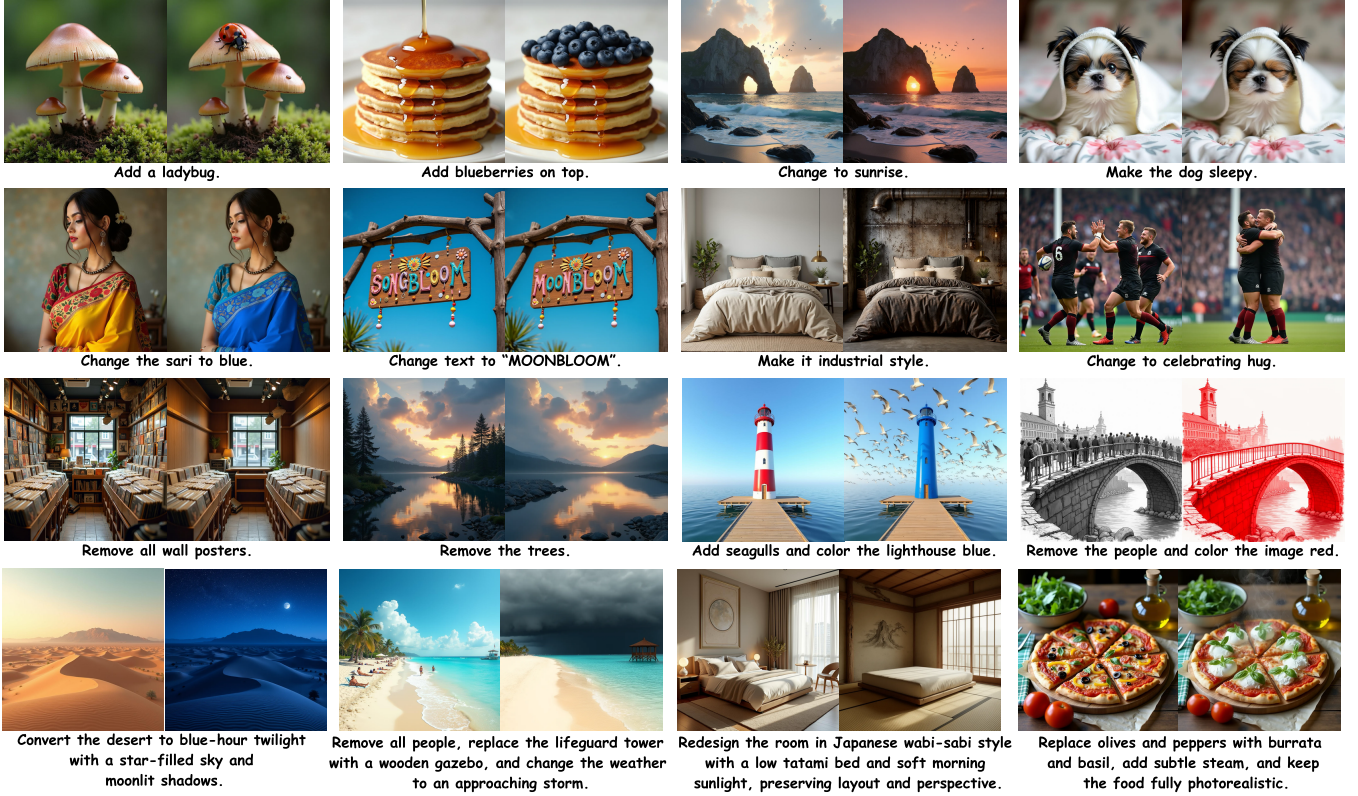


Figure 11: Image editing examples on complex scenarios.

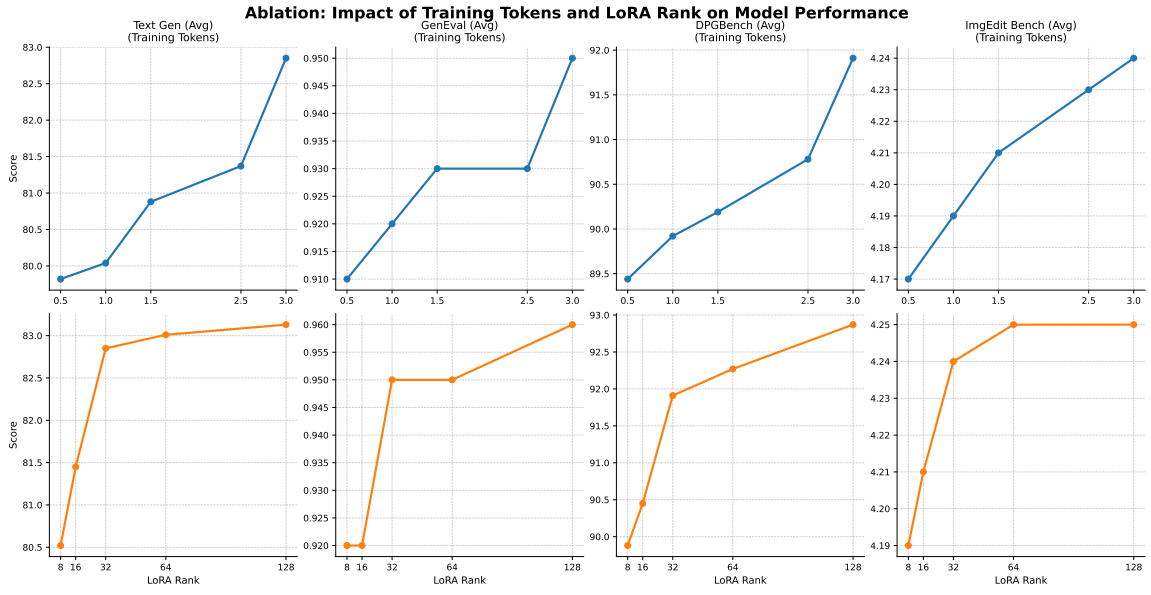


Figure 12: Analysis based on the number of training tokens and LoRA rank used during training.



Figure 13: Image editing on complex scenarios.

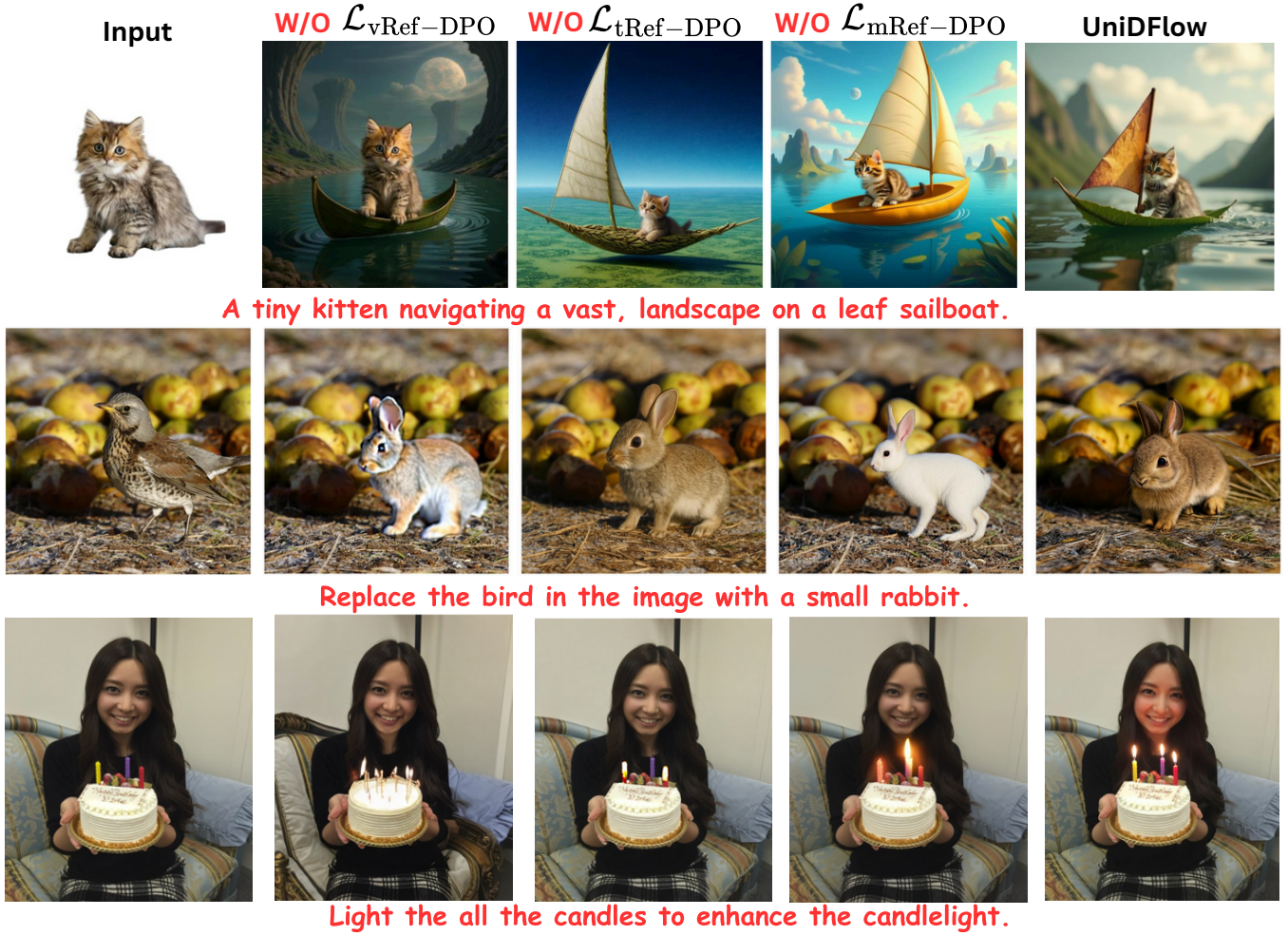


Figure 14: Visual ablation based on Stage-III alignment losses.



A backpack, a suitcase, and sunglasses placed on the ground at a campsite.



A delicious meal featuring roasted chicken wings, sliced ham, and pan-seared chicken drumsticks served together on a wooden table.



A woman sitting indoors, with a vintage lantern and a painter's palette nearby, soft natural light.



Arrange all three reference vases in one image with consistent lighting and a balanced composition.



Pasta, cheesecake, and a modern restaurant interior in one cohesive, realistic scene.

Figure 15: Zero-shot multi-subject reasoning-based editing.



A nighttime neighborhood scene featuring a cozy house, a vintage white car, and a carved pumpkin glowing at dusk.



A cozy indoor workspace with a sleek floor lamp, a laptop on the table, and a curious kitten sitting close by.



A warm, sunlit interior with a cat sitting by the window, a jar of juice, and a beaded bracelet placed casually on a table.



A close-up nature scene featuring a white flower, a butterfly resting nearby, and a blooming white rose.



A rural field scene with rows of corn, a watermelon resting on the soil, and a cucumber growing among young plants.

Figure 16: Zero-shot multi-subject reasoning-based editing.

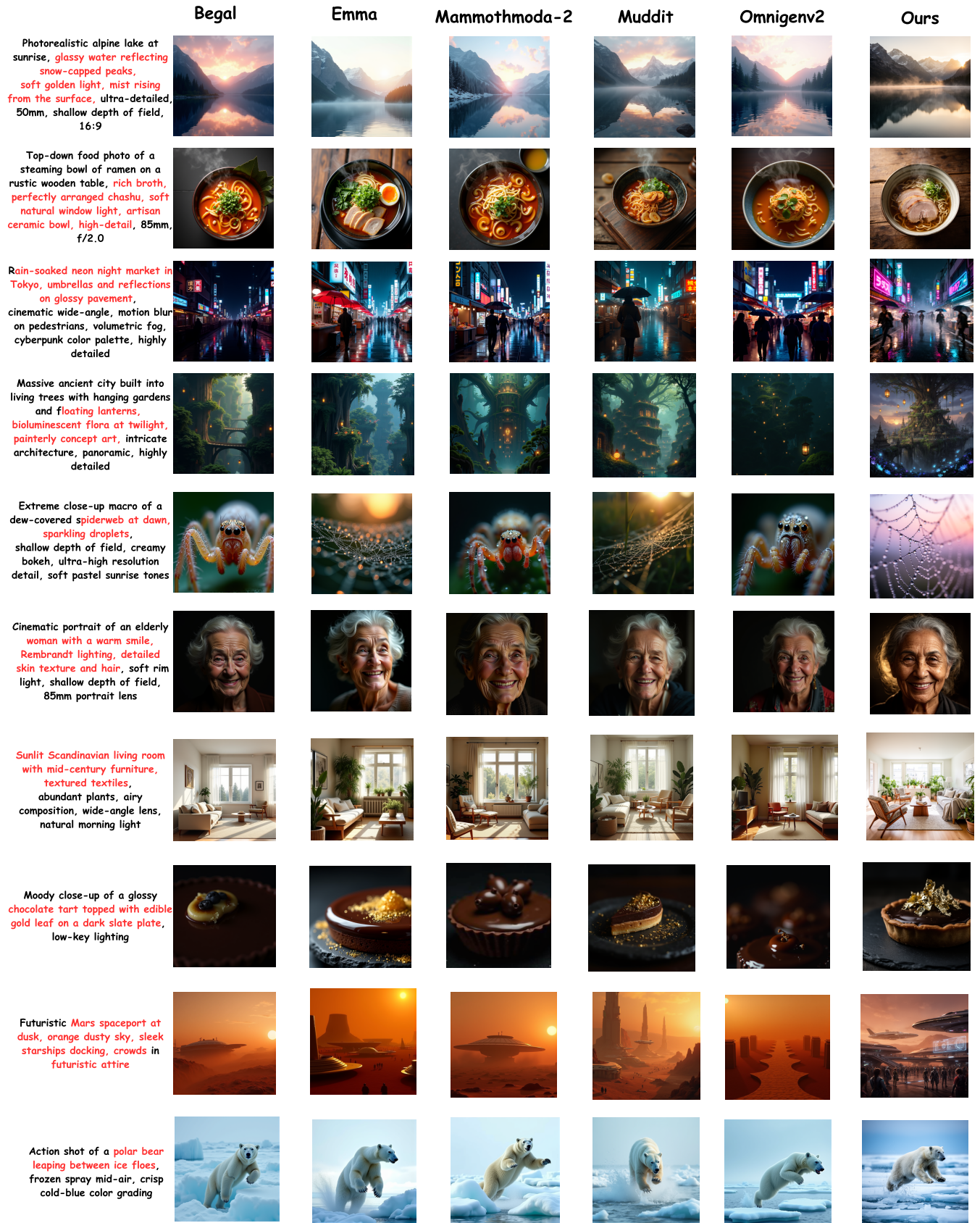


Figure 17: Text-to-Image generation comparison with baselines.

Whats date weather is Shown

Its 14 March 2017

Version:2.0.6

What's new?

- 1)Performance improvements
- 2)Bugs fixed

Cannot find ES File Explorer, it's a featured local and network file manager, ES Task Manager is a module of ES File Explorer and perfectly integrated with it. Do you want to find and install it?

Yes No

What are the new things done in update?

Fixed Bugs, Performance Imporvement

The image shows a small boat with several people on board. If people are preparing for marine travel, appropriate safety equipment should be worn. Describe the scene and determine whether this condition is satisfied.

The image shows a small boat floating on calm water with several people on board. The boat is painted blue and yellow, and the passengers are seated near the cabin area. The people appear to be wearing bright orange life jackets, which are standard marine safety equipment. Based on this, the condition is satisfied, as appropriate safety gear is being worn for marine travel.

What is the name of the app?

NIV Study Bible

Nutrition Facts

Amount/Serving
2/3 cup (89g)

% Daily Value
Total Fat 0g 0%
Saturated Fat 0g 0%
Trans Fat 0g 0%
Cholesterol 0mg 0%
Sodium 0mg 0%
Calories from Fat 0g 0%

Vitamin A 8% • Vitamin C 10% • Calcium 0% • Iron 6%

What is the serving size of the product?

2/3 cup (89g)

Figure 18: Image understanding and reasoning with complex scenes.



Describe the urban street scene shown in this image.



The image shows a busy, sunlit urban street with light traffic and parked vehicles, including several pickup trucks in the foreground. Low-rise buildings sit close to the road, partly shaded by leafy trees, while tall utility poles and a dense web of overhead power lines dominate the skyline. The streetscape is cluttered with prominent storefront and roadside signs in multiple languages, Thai and English on several boards



Describe the urban environment shown in this image.



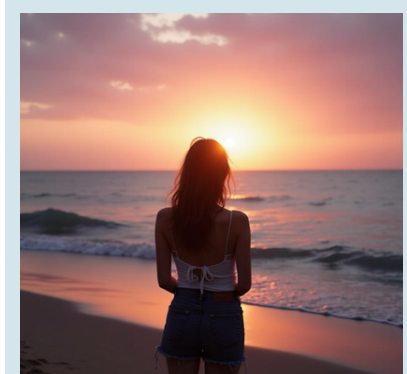
The scene looks like a street-level corner of a city building with a large, grid-framed window revealing the inside of a casual fast-food/caf   space. A strip of signage along the bottom of the window advertises menu items (including "HOT WRAPS"), while a few patrons sit inside at tables. Outside, the building has a heavy stone/concrete facade with a small ventilation grate,



The image shows a person holding sports equipment in a professional outdoor setting. Describe the scene and explain how the equipment and environment suggest the activity taking place.



A player is on a tennis court swinging a racket at a yellow ball. The green hard court, line markings, sponsor boards, and an official seated nearby all indicate a professional tennis match or tournament.



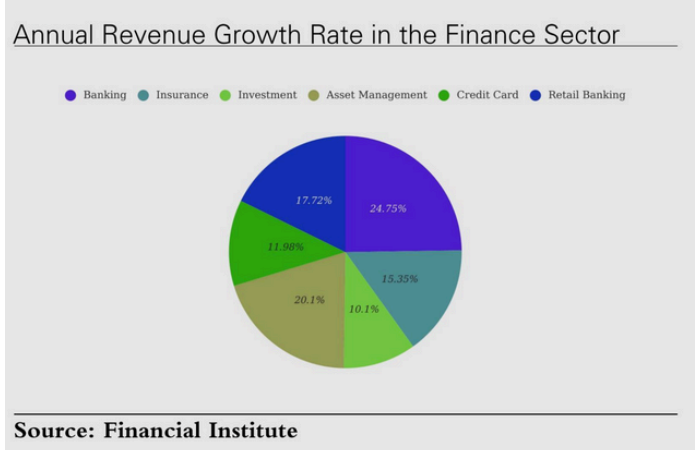
What does costal scene represents ?



It represents peace, reflection, and transition.

A person standing alone on the beach at sunset often symbolizes
Calm and escape from daily life
Introspection
New beginnings or endings

Figure 19: Image-to-text generated results with UniDFlow.



Karl Jenkins
Arranged by Robert Longfield
The Armed Man
(L'Homme armé)
Mvt. I from *The Armed Man: A Mass for Peace*

Instrumentation

1 – Bell Score	2 – F Horn 1
8 – Flute/Piccolo	2 – F Horn 2
2 – Oboe	3 – Trombone 1
2 – Bassoon	3 – Trombone 2
4 – B♭ Clarinet 1	2 – Euphonium B.C.
4 – B♭ Clarinet 2	2 – Euphonium T.C.
4 – C Bassoon	4 – Bass Drums
2 – B♭ Bass Clarinet	1 – String Bass
2 – B♭ Alto Saxophone 1	4 – Percussion 1
2 – B♭ Alto Saxophone 2	1 – Bass Drum (D), Bass Drum, Floor Tom
2 – B♭ Baritone Saxophone	2 – Percussion 2
3 – B♭ Trumpet 1	2 – Percussion 3
3 – B♭ Trumpet 2	Concert Toms (D)
3 – B♭ Trumpet 3	1 – Timpani

Additional Parts U.S. \$1.50
Score (48023736) U.S. \$1.00
BOOSEY & HAWKES
ALFRED L. LEONARD
ALFRED L. LEONARD LTD., LONDON, ENGLAND
© 1982 Boosey & Hawkes Music Ltd.



What is the title of the piece arranged by Robert Longfield?

 **1 Amazing Man**



What is the serving size of the "nutrients" listed on the mug?

 **1 Amazing Man**

what brand of watch is this?

 **invicta**

 Convert the key information in the chart into a nested python dict.

```
{"\"title\": \"Annual Revenue Growth Rate in the Finance Sector\", \"source\": \"Source: Financial Institute\", \"x_title\": \"None\", \"y_title\": \"None\", \"values\": {\"Banking\": \"25.0%\", \"Insurance\": \"15.5%\", \"Investment\": \"12.1%\", \"Asset Management\": \"20.3%\", \"Credit Card\": \"10.1%\", \"Retail Banking\": \"17.9%\"}}}
```



You were served by:
Lesedi Hlongwane

Date	Time	Store	Reg	Txn
04/04/24	05:34 pm	S125	104	0190

Discover the award winning Dis-Chem App! Download it now from Google Play Store | iOS App Store

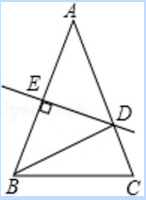
Who served the customer?

 **Lesedi Hlongwane**

Figure 20: Image-to-text generated results with UniDFlow.

Mathematical Geometry

As shown in the figure, angle A = 36.0, then the degree of angle BDC is ()
A. 72° B. 36° C. 60° D. 82°



60

OCR Task

What is written in the image?



Image Caption
describe this image.

A white city bus pulling into a depot on a rainy day, with other buses parked in the background.



Image Understanding

In which of the following types of leaf forms is the blade completely undivided? Palmately Compound Leaf, None, Double Compound Leaf, or Simple Leaf?

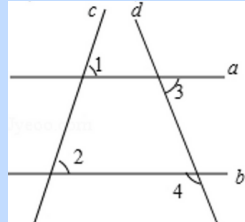


Palmately Compound Leaf

Figure 21: Additional complex reasoning tasks with UniDFlow.

Mathematical Geometry

The positions of straight lines a, b, c, and d are shown in the figure. If angle 1 = 58.0, angle 2 = 58.0, angle 3 = 70.0, then angle 4 is equal to ()
A. 58° B. 70° C. 110° D. 116°



116

OCR Task

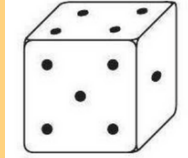
What is written in the image?



Paradise Lions, Saturday farmers MARKet

Mathematical Geometry

How many points are there in the three unseen sides of dice?



Might be 10

Figure 22: Additional complex reasoning tasks with UniDFlow.

Dataset curation prompt used in our pipeline

```

You are an expert data curator for multimodal image-editing instruction datasets.

Inputs:
1) SOURCE_IMAGE: the original image
2) RAW_INSTRUCTION: the original instruction text
3) EDITED_IMAGE: the ground-truth edited image

Tasks:
1) Produce clean training fields.
2) Create preference pairs by writing one "chosen" output and >=3 "rejected" alternatives (plausible but worse).

Rules:
- Preserve intent; if ambiguous, pick the interpretation that matches EDITED_IMAGE.
- Be consistent with what is visible in SOURCE_IMAGE and EDITED_IMAGE; do not invent unseen details.
- Be explicit: what changes, where, how much/style constraints, and what must remain unchanged if relevant.
- Reflection describes the final edited image relative to the original; only observable outcomes.

Rejected alternatives (>=3):
- Each must be a realistic mistake (not nonsense) and include:
  - worse tuned instruction
  - worse edit directive
  - worse reflection of the incorrect outcome
  - "why_rejected" explaining what is wrong vs the chosen
  - "negative_type" from: under-edit, over-edit, wrong-attribute, wrong-region, unwanted-add/remove
- Include at least one near-miss (almost correct but subtly wrong: intensity, shade, lighting, missed constraint).

Output JSON (return ONLY valid JSON; exactly these keys):
{
  "prompt": string,
  "image": "SOURCE_IMAGE",
  "answer_instruction_tuned": string,
  "edit_instruction_for_image": string,
  "edited_image": "EDITED_IMAGE",
  "reflection_of_edited_image": string,
  "preference_data": {
    "prompt": string,
    "chosen": {
      "answer_instruction_tuned": string,
      "edit_instruction_for_image": string,
      "reflection_of_edited_image": string
    },
    "rejected": [
      {
        "answer_instruction_tuned": string,
        "edit_instruction_for_image": string,
        "reflection_of_edited_image": string,
        "why_rejected": string,
        "negative_type": string
      }
    ]
  }
}

Now process:
SOURCE_IMAGE: <<IMAGE>>
RAW_INSTRUCTION: <<INSTRUCTION_TEXT>>
EDITED_IMAGE: <<EDITED_IMAGE>>

```